

# 1 Importance of aerosol composition and mixing state for 2 cloud droplet activation over the Arctic pack ice in summer

3 C. Leck<sup>1</sup> and E. Svensson<sup>1</sup>

4 [1]{Department of Meteorology and Bert Bolin Centre for Climate Research, Stockholm  
5 University, SE-10691 Stockholm, Sweden}

6 Correspondence to: C. Leck ([lina@misu.su.se](mailto:lina@misu.su.se))

## 7 8 **Abstract**

9 Concentrations of cloud condensation nuclei (CCN) were measured throughout an expedition  
10 by icebreaker around the central Arctic Ocean, including a 3-week ice drift operation at 87°N,  
11 from August 3 to September 9, 2008. In agreement with previous observations in the area and  
12 season median daily CCN concentrations at 0.2% water vapor supersaturation were typically  
13 in the range of 15 to 30 cm<sup>-3</sup>, but concentrations varied by two to three orders of magnitude  
14 over the expedition and were occasionally below 1 cm<sup>-3</sup>. The CCN concentrations were  
15 highest near the ice edge and fell by a factor of three in the first 48 hours of transport from the  
16 open sea into the pack ice region. For longer transport times they increased again indicating a  
17 local source over the pack ice, suggested to be polymer gels, via drops injected into the air by  
18 bubbles bursting on open leads. We inferred the properties of the unexplained non-water  
19 soluble aerosol fraction that was necessary for reproducing the observed concentrations of  
20 CCN. This was made possible by assuming Köhler theory and simulating the cloud nucleation  
21 process using a Lagrangian adiabatic air parcel model that solves the kinetic formulation for  
22 condensation of water on size resolved aerosol particles. We propose that the portion of the  
23 internally/externally mixed water insoluble particles was larger in the corresponding smaller  
24 aerosol sizes ranges. These particles were physically and chemically behaving as polymer  
25 gels: the interaction of the hydrophilic and hydrophobic entities on the structures of polymer  
26 gels during cloud droplet activation would at first only show a partial wetting character and  
27 only weak hygroscopic growth. Given time, a high CCN activation efficiency is achieved,  
28 which is promoted by the hydrophilicity or surface-active properties of the gels. Thus the  
29 result in this study argues for that the behavior of the high Arctic aerosol in CCN-counters

1 operating at water vapor supersaturations  $> 0.4 \%$  (high relative humidities) may not be  
2 properly explained by conventional Köhler theory.

3

#### 4 **1 Introduction**

5 Twomey (1974) showed that the state of division of the available water in clouds determines  
6 the amount of short wave radiation scattered back to space, the effect being largest in  
7 optically thin clouds with few water drops. This is particular true for Arctic low-level clouds  
8 (Walsh et al., 2002; Tjernström et al., 2008). Further these Arctic low-level clouds, while  
9 controlling the surface radiation balance, have a pronounced influence on the melting and  
10 freezing of the perennial sea ice (Intrieri, 2002; Kay and Gettelman, 2009; Mauritsen et al.,  
11 2010; Sedlar et a., 2011). For most of the year, such clouds tend to warm the surface, but  
12 during the peak melt season at the end of the summer, low-level clouds could cool the ice  
13 surface and thereby influence the timing of the autumn freeze-up. Earlier freeze-up will cause  
14 thicker ice that might melt less during the following summer, surviving into the subsequent  
15 winter. If such a process were to recur over several years, it could delay or even prevent sea  
16 ice from melting completely during the Arctic summer. In other words, it would constitute a  
17 negative feedback. The concentration of cloud water drops is largely determined by the  
18 concentration of nuclei on which cloud drops can form (cloud condensation nuclei, or CCN).  
19 This also requires that the meteorological conditions, wind, humidity and temperature are  
20 favorable.

21 Measurements of cloud condensation number concentrations (CCNC) over the pack ice are  
22 scarce due to the remoteness of the area. From research carried out in a series of four  
23 international ice-breaker expeditions to the high Arctic in the summers of 1991 (Leck et al.,  
24 1996), 1996 (Leck et al., 2001), and 2001 (Leck et al., 2004; Tjernström et al., 2004) and in  
25 2008 (Tjernström et al., 2014) there has been no other effort relevant to the formation of low-  
26 level clouds, north of  $80^\circ$ , during conditions when influences from man-made particle sources  
27 being limited. CCNC have been observed to vary by three orders of magnitude over the  
28 period July to September and commonly by an order of magnitude within a day but were  
29 usually lower than  $100 \text{ cm}^{-3}$ , occasionally less than  $1 \text{ cm}^{-3}$  (Lannefors et al., 1983; Bigg et al.,  
30 1996:2001; Bigg and Leck, 2001a; Leck et al., 2002; Mauritsen et al., 2011). Figure 6 in  
31 Mauritsen et al. displays frequency distributions of observed CCNC from all four expeditions  
32 measured at different water vapor supersaturations (SS), ranging 0.1 to 0.8 %. All four

1 populations showed an overall consistent distribution with three quarters of the CCNC being  
2 greater than  $10 \text{ cm}^{-3}$  but less than about  $100 \text{ cm}^{-3}$ , medians typically in the range 15 to  $50 \text{ cm}^{-3}$   
3 as reported by Bigg et al. (1996) and Bigg and Leck (2001a).

4 In searching for a relationship between the properties of the summer high Arctic aerosol and  
5 its ability to form CCN, Zhou et al. (2001) calculated CCNC by assuming equilibrium Köhler  
6 theory (Köhler, 1936). The calculations used aerosol number size distribution data and  
7 additional hygroscopic growth information and assumed that the calculated CCN particles  
8 were composed of ammonium sulfate, sodium chloride and a nearly water-insoluble fraction.

9 The closure study resulted in an over-prediction of the calculated CCNC (more CCN were  
10 calculated than measured) of around 30%. In a separate study on the same CCN data Bigg and  
11 Leck (2001a) made the simpler assumption that all particles in the number size distribution  
12 were composed of pure ammonium sulfate. Again a similar over-prediction resulted as  
13 reported by Zhou et al. (2001). Sorting the CCN data according to meteorological conditions  
14 combined with added information on particle morphology and state of mixture Leck et al.  
15 (2002) concluded that other components, probably organics, depressed the nucleating ability  
16 of the particles. However, on clear-sky days, there were a majority of occasions on which  
17 observed CCNC were higher than predicted from a sulfate composition and the measured size  
18 distribution. Since equilibrium Köhler theory cannot take kinetic effects into account, which  
19 can cause erroneous results when considering the competition of aerosol particles of different  
20 size for water vapor, the cloud nucleation process was in addition simulated with a  
21 Lagrangian parcel model (Lohmann and Leck, 2005). In order to explain the observed CCNC  
22 over the pack ice the authors found it necessary to invoke an Aitken mode composed of  
23 highly surface-active organics, externally mixed with a sulfur-containing population. Most  
24 recently Martin et al. (2011) performed yet another CCN closure study being representative  
25 for high Arctic summer conditions. To predict the CCNC, the closure was based on data on  
26 average measured from 0.1% to 0.7% water vapor SS and  $\kappa$ -Köhler theory (Petters and  
27 Kreidenweis, 2007). This approach differed from the previous studies which only used one  
28 level of water vapor SS (0.2%) in the comparison between measured and modeled CCNC.  
29 Further Martin et al. used highly time resolved (average over 5 minutes) sub-micrometer  
30 aerosol bulk chemical compositions (sulfate, nitrate, organics and methane sulfonate)  
31 obtained by an aerosol mass spectrometer, see Chang et al. (2011) for details. The authors  
32 derived total hygroscopicity parameters by permuting parameter values for the components

1 and the solubility of the organics. The surface tension was assumed to be constant and equal  
2 to that of pure water. Consistent with the previous results by Zou et al. (2001) and Bigg and  
3 Leck (2001a), the calculations generally tended to over predict the observed CCNC, with  
4 about 30-60% for water vapor SS above 0.4%. To explain the results the authors proposed  
5 that the portion of the particles assumed to be made up by internally mixed water insoluble  
6 organics, was larger in for the smaller sizes ranges. The above discussed opposing CCN-  
7 closure results indicate that the observed presence of organic constituents, possibly both  
8 marine primary and secondary, most likely will play an important role in determining the  
9 ability of the aerosol collected over the Arctic pack ice area to act as CCN.

10 This study will attempt to further reduce some of the uncertainties surrounding the CCN  
11 properties promoting/suppressing cloud droplet formation over the Arctic pack ice area with  
12 limited influences from man-made activities. This will be made possible by using observed  
13 sensitivity (on average between 0.1 to 0.7 % water vapor SS) of measured CCNC combined  
14 with Köhler theory and by simulating the cloud nucleation process using a Lagrangian  
15 adiabatic air parcel model that solves the kinetic formulation for condensation of water on  
16 size resolved aerosol particles. The simulations will be based on the diffusional growth  
17 equation as was used in Lohmann and Leck (2005). The CCNC will be predicted from  
18 observed aerosol number size distribution data and additional hygroscopic growth  
19 information, and by assuming that the calculated CCN particles were composed of an  
20 inorganic/organic aerosol system. In the latter case we will use the determined aerosol bulk  
21 chemistry obtained from highly size resolved impactor samples to show the extent to which  
22 determined water-soluble dimethyl sulfide (DMS) oxidation products, sodium chloride and  
23 other inorganic compounds contributed to the CCN population. As a surrogate for the  
24 unexplained fraction assumed to be organic in nature we will use various water-soluble,  
25 slightly water-soluble and non water-soluble proxy constituents. The simulated CCNC will be  
26 compared to the observed CCNC, at water vapor SS on average ranging between 0.1 to 0.7%,  
27 collected during the Arctic Summer Cloud Ocean Study (ASCOS)<sup>1</sup> onboard the Swedish  
28 icebreaker *Oden* in 2008 in the open waters and marginal ice zone of the Greenland Sea –  
29 Fram Strait area and over the pack ice north of 80°. For detailed information on the quality

---

<sup>1</sup> The interdisciplinary program of ASCOS was conducted in the fields of marine biology and chemistry, atmospheric chemistry, oceanography and meteorology with the overall aim to improve our understanding of low-level cloud formation and possible climate feedback processes over the central Arctic Ocean. Tjernström et al., 2014 give more details.

1 and data processing of the measurements of CCN, aerosol number size distributions and  
2 aerosol hygroscopic growth we refer to Martin et al. (2011), Heintzenberg and Leck (2012)  
3 and Zou et al. (2001).

## 4 5 **2 Rout of the expedition and measuring systems and methods**

### 6 **2.1 Rout and platform**

7 The CCNC simulations presented here utilize measurements carried out onboard the  
8 icebreaker *Oden* as part of ASCOS. Samples were collected in surface air over the central  
9 Arctic Ocean during the biologically most active summer period. The expedition departed  
10 from Longyearbyen, Svalbard on 2 August 2008 (Day Of Year, DOY 215, note the leap year),  
11 and headed north for the pack ice of the central Arctic Ocean. There was a transition from the  
12 “marginal ice zone” having 20-70% ice cover and the “pack ice region” having between 80%-  
13 95% ice cover. On 12 August (DOY 225) *Oden* was anchored to a large ice floe, slightly  
14 north of 87°N, and proceeded to drift with the ice floe for the following three weeks (referred  
15 to as the Pack Ice, PI, -drift), until midnight between 1 and 2 September (DOY 245-246). In  
16 transit to the ice drift, additional stations were set up at the ice edge and an open water station  
17 in the Greenland Sea – Fram Strait area: an open water station (OW-1) on the 3<sup>rd</sup> of August  
18 2008 (DOY 216-216.5) (78.2° N; 7.5° E) followed by a station in the marginal ice zone (MIZ-  
19 1) starting on the 4<sup>th</sup> of August 2008 (DOY 217.5) (79.9° N; 6.1° E). On the way back from  
20 the ice drift, a second marginal ice edge station (MIZ-2) was set up at the ice edge on the 6<sup>th</sup>  
21 of September immediately followed by a final open water station (OW-2) ending on the 7<sup>th</sup> in  
22 the Greenland Sea. As several of the instruments were not in use no data from the MIZ2 and  
23 OW2 stations are discussed in this study. *Oden* arrived back at Longyearbyen on 9 September  
24 (DOY 253). A map of the route with the ice drift magnified is shown in Fig. 1. All times are  
25 reported in Universal Time Coordinate (UTC). The sun was continuously above the horizon  
26 of the expedition.

### 27 **2.2 Particle measurement systems**

28 The measurements utilized in this study were made from a sampling manifold with an  
29 impactor (Anderson Inc., Atlanta, Ga) 50% cutoff diameter of 10 µm (PM<sub>10</sub>) at 25-m height  
30 onboard *Oden*. The PM10 inlet was identical to the one used during all three previous

1 expeditions in the summers of 1991, 1996 and 2001. Direct contamination from the ship was  
2 excluded by using a pollution controller, turning off all the pumps of the samplers, in direct  
3 connection to the sampling manifold. To maximize sampling time safe from pollution our  
4 strategy was to keep the sampling manifold facing upwind to avoid sampling of ship exhausts.  
5 This necessitated a “harbor” in the ice in which the ship, with its non-rotating mast on the 4<sup>th</sup>  
6 deck, could be moored in several different directions and turned as the wind direction  
7 changed. Further details of the location and properties of air intakes and instruments, position  
8 on the ship, pumping arrangements and precautions to exclude contaminated periods can be  
9 found in Leck et al. (2001) and in Tjernström et al. (2014). Key instruments used and  
10 important measurement details are discussed below.

11 (1) Aerosol particles that are active as CCN were measured continuously using two identical  
12 CCN counters (Roberts and Nenes, 2005) operating in parallel. Aerosol particles enter the  
13 CCN counter through an inlet at the top and pass through a cylindrical column where they can  
14 activate and grow to droplet size. In the column a temperature gradient is established, with the  
15 lowest temperature at the top. The walls of this column are wetted with water. Thus, heat and  
16 water vapor are transported towards the center of the column by diffusion. As heat diffuses  
17 more slowly than water in air in the temperature range used, a constant water vapor  
18 supersaturation (SS) is established in the center of the column. This supersaturation can be  
19 adjusted by changing the temperature gradient of the column. At the outlet of the column the  
20 activated particles are counted with an optical particle counter (OPC) and collected in  
21 different size bins. The CCN counter defines a CCN as a particle having a wet diameter  $>$   
22  $1\mu\text{m}$  and a positive growth rate. The CCN counter undercounts particles if they have not  
23 grown larger than  $1\mu\text{m}$  by the time they reach the OPC.

24 The first CCN counter was set to a constant water vapor SS of ca. 0.2% averaged over one  
25 minute, which was slightly increased later for better comparison with CCN data collected  
26 during the three former expeditions: measurements were performed at 0.17% SS between  
27 August 3 (DOY 216) to August 15 (DOY 228) and at 0.21% SS for the remaining period  
28 August 16 (DOY 229) to September 9 (DOY 253). The second counter scanned five different  
29 water vapor SS, on average ranging between 0.1 to 0.7%. After each calibration the settings  
30 of the second counter were adjusted. Therefore, the water vapor SS at which the CCNC were  
31 measured varies for different time periods, with a measurement period of 30 min each. The  
32 average values in percent are given in italic and the spread in brackets: *0.10* (0.082-0.106),

1 0.15 (0.126-0.161), 0.20 (0.171-0.233), 0.41 (0.347-0.521), 0.73 (0.613-0.952). This enabled  
2 a determination of the sensitivity of measured CCN to the choice of water vapor SS. Martin et  
3 al. (2011) give more information on the quality and data processing of the CCNC  
4 measurements.

5 (2) Aerosol particle number size distributions at 10 to 20-min time resolution were measured  
6 in 45 bins from 3 to 800 nm in diameter using a Twin Differential Mobility Particle Sizer  
7 (TDMPS; Birmilli et al., 1999). Throughout this paper all number particle sizes will be  
8 referred to as dry geometric mean diameters (GMD). In the discussion to follow we will refer  
9 to the following modal GMD representation of the observations: the Aitken mode (25-70 nm),  
10 the accumulation mode (70-1000 nm) and recently nucleated mode (< 10nm). Table 1 shows  
11 examples of the particle number variability seen by the TDMPS during the duration of the  
12 impactors. Tabulated are the 25<sup>th</sup>, 50<sup>th</sup> (median) and 75<sup>th</sup> percentile aerosol number  
13 concentrations for 40 nm, 80 nm and 300 nm diameters, respectively. Further details on the  
14 quality and data processing of these measurements are available in Heintzenberg and Leck  
15 (2012).

16 (3) To measure the growth of individual particles in diameter sizes of 31, 50, 72, 108, 163 and  
17 263 nm from the dry state (<20 % RH) to a set RH, an H-TDMA (Hygroscopic Tandem  
18 Differential Mobility Analyzer) instrument was used. Zhou et al. (2001) gives details.

19 (4) Aerosol bulk chemical composition was determined from a 13-stage (30 dm<sup>3</sup> min<sup>-1</sup>), LPI  
20 (Dekati, <http://dekati.com/cms/>) impactor. Upstream of the impactor, the temperature and the  
21 RH (on average 40%) of the incoming sample air were measured and recorded using mini  
22 probes and a data acquisition system custom made for the expedition by Vaisala. The LPI  
23 impactor had 50% cut off diameters of: 10.0, 6.57, 3.96, 2.45, 1.60, 0.990, 0.634, 0.391,  
24 0.253, 0.165, 0.104, 0.060 and 0.029  $\mu\text{m}$  aerodynamic diameter (EAD). Polycarbonate  
25 collection foils were used as the collection substrate. The impaction stages 1 (10.0 - 6.57  $\mu\text{m}$   
26 EAD), 2 (6.57 - 3.96  $\mu\text{m}$  EAD) and 3 (3.96 - 2.45  $\mu\text{m}$  EAD) at the inlet of the impactor were  
27 coated with grease (Apiezon-L dissolved in hexane) to prevent the bounce-off of larger  
28 particles with their relatively large masses onto the downstream stages. The amount of mass,  
29 if any, bounced from upper stages is difficult to quantify. However, the fact that sodium  
30 concentration in the submicron stages did not systematically follow the supermicron sodium  
31 concentration is an indirect indication that the substrate greasing was sufficient to reduce or  
32 eliminate serious bounce-off. Blank levels were determined by loading 6 impactors with the

1 substrates at the sampling site for the length of the sampling period but with no air drawn  
2 through it. The detailed size segregated LPI impactor required relative long sampling times of  
3 20-40 hours resulting in 18 sampling periods obtained during the course of ASCOS.

### 4 **2.3 Water soluble mass determination**

5 To allow for subsequent chemical determinations all substrates, ambient samples and blanks  
6 were carefully handled in a glove box (free from particles, sulfur dioxide and ammonia) both  
7 prior to and after sampling. At the time of the chemical analyses, still in the glove box, the  
8 substrates were extracted (in centrifuge tubes) with 5 cm<sup>3</sup> deionized water (Millipore Alpha-  
9 Q, conductivity 18 MΩcm). For sufficient extraction the substrate extracts were finally placed  
10 in an ultra sonic bath for 60 min. The extracts were then analyzed for major cations, anions  
11 and weak anions by chemically suppressed ion chromatography (IC, Dionex ICS-2000). The  
12 anions were analyzed with Dionex AG11/AS11 columns and the cations with CG16/CS16. A  
13 Dionex ATC-1 column was used before the injection valve to trap carbonates and other ionic  
14 contaminants. The injection volume was 50 μdm<sup>3</sup>. Quality checks of the IC-analyses were  
15 performed with both internal and external reference samples (organized by EANET, 2008).  
16 Systematic errors were less than 2% (with exception for magnesium, Mg<sup>2+</sup>, with less than 3%)  
17 for all ionic components. The analytical detection limits obtained for the various ions, defined  
18 as twice the level of peak-to-peak instrument noise, were 0.20, 0.05, 0.01, 0.01, 0.01 and 0.05,  
19 0.00, 0.00, 0.02, and 0.01 μeq dm<sup>-3</sup> for ammonium: NH<sup>+</sup><sub>4</sub>, sodium: Na<sup>+</sup>, potassium: K<sup>+</sup>,  
20 magnesium: Mg<sup>2+</sup> and calcium: Ca<sup>2+</sup>, chloride: Cl<sup>-</sup>, MSA: CH<sub>3</sub>SOO<sup>-</sup>, oxalate: C<sub>2</sub>O<sub>4</sub><sup>2-</sup>, nitrate:  
21 NO<sub>3</sub><sup>-</sup> and sulfate: SO<sub>4</sub><sup>2-</sup>, respectively. The overall analytical accuracy was better than 3% and  
22 5% for the anions and cations, respectively.

23 Blank levels were determined by loading 6 impactors with: 60 (6 impactors each 10 stages)  
24 non greased substrates and 18 (6 impactors each 3 stages) greased substrates. The blank  
25 values for the non-greased impactors obtained for the various ions, defined as average and 1σ  
26 were 0.20±0.03, 0.13±0.02, 0.02±0.007, 0.02±0.005 and 0.12±0.04, 0.14±0.02, 0.00±0.00,  
27 0.00±0.00, 0.06±0.01, and 0.10±0.01 μeq dm<sup>-3</sup> for NH<sup>+</sup><sub>4</sub>, Na<sup>+</sup>, K<sup>+</sup>, Mg<sup>2+</sup> and Ca<sup>2+</sup>, Cl<sup>-</sup>, MSA,  
28 C<sub>2</sub>O<sub>4</sub><sup>2-</sup>, NO<sub>3</sub><sup>-</sup> and SO<sub>4</sub><sup>2-</sup>, respectively. The corresponding values for the greased substrates  
29 were: 0.29±0.03, 0.80±0.16, 0.03±0.004, 0.08±0.005 and 0.29±0.04, 0.22±0.05, 0.00±0.00,  
30 0.00±0.00, 0.10±0.01 and 0.13±0.03 μeq dm<sup>-3</sup> for NH<sup>+</sup><sub>4</sub>, Na<sup>+</sup>, K<sup>+</sup>, Mg<sup>2+</sup> and Ca<sup>2+</sup>, Cl<sup>-</sup>, MSA,  
31 C<sub>2</sub>O<sub>4</sub><sup>2-</sup>, NO<sub>3</sub><sup>-</sup> and SO<sub>4</sub><sup>2-</sup>, respectively.



1 During the expedition LPI levels (sample minus blank) of MSA,  $\text{Cl}^-$ ,  $\text{NO}_3^-$ ,  $\text{SO}_4^{2-}$ , Oxalate,  
2  $\text{Na}^+$ ,  $\text{K}^+$ ,  $\text{Mg}^{2+}$  and  $\text{Ca}^{2+}$  down to 0.002, 0.030, 0.009, 0.010, 0.007, 0.030, 0.004, 0.008, and  
3  $0.032 \text{ nmol m}^{-3}$ , respectively were detected.

#### 4 **2.4 Converting the aerosol chemical mass distributions to aerosol chemical** 5 **number size distributions**

6 The size resolved chemical mass concentration was converted to a chemical number size  
7 distribution by firstly transpose the LPI impactor 50% cut off diameters (EAD at 40% RH) to  
8 dry (20% RH) GMD. Following the assumptions made in Hinds (1999) and Tang and  
9 Munkelwitz (1994) the following dry GMD's resulted: 0.019-0.40  $\mu\text{m}$  (bin-1), 0.40-0.71  $\mu\text{m}$   
10 (bin-2), 0.71-0.116  $\mu\text{m}$  (bin-3), 0.116-0.181  $\mu\text{m}$  (bin-4), 0.181-0.284  $\mu\text{m}$  (bin-5), 0.284-0.466  
11  $\mu\text{m}$  (bin-6), 0.466-0.732  $\mu\text{m}$  (bin-7), 0.732-1.19  $\mu\text{m}$  (bin-8), 1.19-1.82  $\mu\text{m}$  (bin-9), 1.82-2.95  
12  $\mu\text{m}$  (bin-10), 2.95-4.91  $\mu\text{m}$  (bin-11), 4.91-7.59  $\mu\text{m}$  (bin-12)  $\mu\text{m}$ . A size-dependent particle  
13 density (on average  $1.35 \text{ g cm}^{-3}$ ) was calculated assuming mixtures of mainly sea salt,  
14 ammonium sulfate and MSA with smaller amounts of oxalate, potassium, calcium,  
15 magnesium and water similar to those observed. By varying only the average density between  
16  $1.2$  to  $1.4 \text{ g cm}^{-3}$  the uncertainty in the transposed EAD to GMD was estimated to be about  $\pm 5$   
17 %. To reduce the calculated GMD from 40% to 20% RH an observed hygroscopic growth  
18 factors of 1.15 was used. If the we assume an  $\pm 10$  % uncertainty in the observed hygroscopic  
19 growth factors and add the  $\pm 5$  % uncertainties from the density estimates the overall  
20 uncertainty in the transpose from EAD at 40% RH to dry GMD is  $\pm 11$  %. Thereafter we  
21 interpolated the water-soluble mass composition for each of the impactor bins (1-7) to the  
22 TDMPS bins within the 20 to 800 nm diameter size range. The mass concentrations were  
23 then converted to number concentrations. Since the mass to number conversion depends on  
24 the cube of the diameter, the uncertainty of the values resulting from the conversion ranged  
25 between 70-140 %.

#### 26 **2.5 Air trajectories and time spent over the pack ice**

27 The vertical structure of the atmosphere was typical for central Arctic summer during the  
28 expedition. The air layer closest to surface was shallow and well mixed with depths usually  
29 below 200 m. This layer was capped by a temperature inversion with a stable stratification of  
30 the atmosphere aloft due to the advection of warmer air from the south (Tjernström et al.,

1 2012). The backward trajectories were calculated<sup>2</sup> for an arrival height in the well-mixed  
2 layer within the ABL, 100 m above surface level, at hourly intervals. The height of 100 m is a  
3 compromise to ensure that at least the receptor point is fairly close to the surface where the  
4 samples were collected (25 m above sea level), and at least in the well-mixed layer but also  
5 that trajectories, due to rounding errors and interpolation, would not run too great a risk to "hit  
6 the surface" in the backward trajectory calculations. To use *Oden*'s position as a starting point  
7 of the backward trajectory calculations gave a point that is very precisely measured with GPS.  
8 Backward trajectories have several sources of uncertainty, which generally grows with the  
9 length of the trajectory. Most uncertain is transport in the vicinity of strong gradients, such as  
10 frontal zones, while within a single air mass the trajectory calculations are likely more  
11 reliable.

12 With the help of the back-trajectories and ice maps<sup>3</sup> the time elapsed since the air was last in  
13 contact with the open ocean was computed in the way that Nilsson (1996) reported. It will be  
14 referred to as days over ice (DOI). The calculated DOI thus marks the end point for an air  
15 parcel that left the ice edge between 0-10 days ago (resolved by the length of the trajectories).  
16 The measure of DOI will in the later analyses be used as a simple parameter to summarize the  
17 evolution of the aerosol as a function of the synoptic scale systems since their last contact  
18 with open sea. Calculated cumulative travel times over ice for ASCOS, showed that most  
19 trajectories spent at least three days (median 3.3 days) over the pack ice before reaching  
20 *Oden*. Travel times less than two days were encountered around 30% and travel times of four  
21 days and longer covered about 40% of the cases.

22

---

<sup>2</sup> The NOAA HYSPLIT (Hybrid Single-Particle Lagrangian Integrated Trajectory) model (Draxler and Rolph, 2011; Rolph, 2011) was used to calculate three-dimensional five and ten day backward trajectories of the air reaching *Oden*'s position. The trajectory calculations were based on data from the Global Data Assimilation System (GDAS) of the National Weather Service's National Center for Environmental Prediction (NCEP). Vertical motion in the trajectory runs was calculated using the model's vertical velocity fields.

<sup>3</sup> Ice maps from Satellite-sensor, AMSR-E, "level 1A" with the data sourced from NSIDC (Boulder), United States, finalized at Bremen University, <http://iup.physik.uni-bremen.de:8084/amsr/amsre.html> were used.

### 1    **3 Computational methodes**

2 Köhler (1936) describes the relationship between chemical properties, size and water vapor  
3 supersaturation present at the surface of an aerosol droplet in thermodynamic equilibrium.  
4 The Köhler theory consists of the Kelvin effect, which describes the influence on water vapor  
5 SS pressure from the curvature of the spherical surface of an aerosol droplet, and the Raoult  
6 effect, which represents the influence from the solute. One key parameter in the Kelvin term  
7 is the surface tension. The surface tension of an aerosol particle is not only influenced by the  
8 curvature of the droplet but also determined by the concentration of amphiphilic solutes  
9 (Hede et al., 2011). Thus inorganic salts could be assumed to have an increasing effect on  
10 surface tension due to the ionic interactions, whereas surface-active organic compounds  
11 decrease the surface tension due to the amphiphilic properties disturbing the hydrogen  
12 bonding at the air/water interface. If a thermodynamic equilibrium with the environment of  
13 the aerosol droplet can be assumed the droplet diameter size of a growing CCN particle can  
14 be calculated at a specific water vapor SS pressure. In the simplest use of the traditional  
15 Köhler theory keeping all parameters constant, the larger the aerosol droplet diameter is, the  
16 lower critical water vapor SS pressure is required for final activation into a cloud droplet.

17 The water vapor SS pressure over an aqueous aerosol droplet can also be expressed to depend  
18 on the droplet water activity ( $a_w$ ) according to:

$$19 \quad SS = a_w \exp(4\sigma_{s/a} M_w / RT \delta_w D), \quad (1)$$

20 where  $\sigma_{s/a}$  is the surface tension between the solution and air,  $M_w$  is the molecular weight of  
21 the water solution,  $\delta_w$  the density of the solution,  $R$  is the universal gas constant,  $T$  is the  
22 absolute temperature and  $D$  is the diameter of the droplet at the water vapor SS pressure. The  
23 droplet water activity,  $a_w$ , is a straightforward parameter, which can be measured directly in  
24 laboratory experiments. Svenningsson et al. (2006) measured water activities as functions of  
25 solution molality for various mixtures of inorganic and organic compounds, and gave  
26 parameterizations. In this study we have used the MIXSEA mixture (ammonium sulfate 50%,  
27 sodium chloride 30%, succinic acid 10% and fulvic acid 10%) parameterization.

28 The above formula (1) can be reformulated using  $\kappa$ -Köhler theory (Petters and Kreidenweis,  
29 2007).  $\kappa$ -Köhler theory is a one-parameter model, where the solute hygroscopicity parameter,  
30  $\kappa$ , combined with the Kelvin term represents a measure of aerosol droplet water uptake and  
31 activity and thus determines the equilibrium water vapor SS over an aqueous droplet. Values

1 of  $\kappa$  for specific constituents, or mixtures thereof, can be determined experimentally. Fitted  
2 values of  $\kappa$  for individual aerosol constituents may be combined to represent the hygroscopic  
3 behavior of mixed aerosol particles of known composition. The water vapor SS pressure over  
4 an aqueous aerosol droplet could in this case be expressed as:

$$5 \quad SS = D^3 - D_d^3 / D^3 - D_d^3 (1 - \kappa) \exp(4\sigma_{s/a} M_w / RT \delta_w D), \quad (2)$$

6 where  $D_d$  is the volume equivalent diameter of the dry aerosol particle.  $\kappa$  depends on the  
7 water activity of the aerosol droplet and the volumes of the dry particle and of the aerosol  
8 droplet. It ranges between 0 for water-insoluble particles, and values  $> 1$  for very water  
9 soluble salts ( $\kappa = 1.28$  for NaCl).  $\kappa$  of an aerosol droplet is defined as the sum of the products  
10 of the  $\kappa$  values of all single solute components,  $i$ , in the aerosol droplet and their  
11 corresponding volume fractions  $\epsilon_i = V_i / V_{tot}$ , thus  $\kappa_{tot} = \sum_i \kappa_i \epsilon_i$ . To calculate  $\kappa_{tot}$ ,  $\kappa$  values  
12 and densities for the separate mass constituents measured by the impactors had to be assumed.  
13 As with traditional Köhler theory, the maximum in water vapor SS computed for a specified  
14 initial dry particle size (referred to as the activation limit dry diameter) and composition  
15 (expressed by  $\kappa$ ) determines the particle's critical water vapor supersaturation (SSc) for  
16 activation to a cloud droplet.

17 Since equilibrium Köhler theory cannot take kinetic effects into account, which can cause  
18 erroneous results when considering the competition of aerosol particles of different size for  
19 water vapor, we simulated the cloud nucleation process by assuming Köhler theory combined  
20 with a Lagrangian adiabatic air parcel model (coded in Matlab). The model, which is  
21 described by Pruppacher and Klett (1997), solves the kinetic formulation for condensation of  
22 water on size resolved aerosol particles, based on the diffusional growth equation. The model  
23 is composed of essentially the same equations as the model developed in Leaitch et al. (1986)  
24 and later applied by Lohman and Leck (2005), but for a few differences. Firstly, due to  
25 development of both computer hard- and software it is now possible to solve the full implicit  
26 ordinary differential equation system instead of earlier necessary simplifications. Secondly,  
27 measured size distributions of both number and chemical compositions are used as direct  
28 model input variables. The main advantage of this approach is that the observed mass and  
29 number aerosol size distributions are preserved. In the **Leaitch** et al. and Lohman and Leck  
30 studies the size distributions had to be transferred to a series of log-normal distributions with  
31 constant chemical composition, which caused a risk for loss of size resolved information.

1 However the uncertainty in mass that arises from the chemical analyses (section 2.3) together  
2 with uncertainties connected with the measured growth factors (section 2.4) still could  
3 influence our results. This is reflected in the shown error bars of Figures 11 and 12. Finally,  
4 we identify that the Raoult term in the particle growth equation given in the Supplementary  
5 material is equal to  $-\ln(a_w)$ . Similar to Lohmann and Leck (2005) the model defines a CCN as  
6 a particle having a wet diameter  $> 1\mu\text{m}$  and a positive growth rate. The total simulation length  
7 was 50 s and set to correspond to the residence time of the particles in the CCN counter. For  
8 more detailed information on the modeling approach we refer to the information in  
9 Supplementary material.

## 11 4 Results of CCN measurements

### 12 4.1 Temporal changes of CCNC

13 Figure 2 gives a time series of the CCN observations (averaged over one minute) for water  
14 vapor SS of 0.2% (sampler 1). Blue dots show CCNC measured at 0.17% SS (DOY 216-228),  
15 while light blue dots show the CCNC at 0.21% SS (DOY 229-253). Between days 216 and  
16 218 the measurements were collected in the open sea or at the marginal ice edge of the  
17 Greenland Sea – Fram Strait area. The period between DOY 225 to 246 represents the ice  
18 drift period. Four features stand out: The CCNC were constantly below  $100\text{ cm}^{-3}$  both in the  
19 marginal over the pack ice, and occasionally below  $1\text{ cm}^{-3}$  (described in Mauritzen et al.,  
20 2010), the 2-3 orders of magnitude overall range in concentrations from below  $1\text{-}100\text{ cm}^{-3}$  and  
21 changes in concentration, sometimes exceeding the entire seasonal variation, often occurred  
22 within an hour. This large temporal variability in the data is consistent with measurements  
23 from earlier high Arctic campaigns. Work by Bigg et al., 2001 has shown that the common  
24 stratification together with dynamic processes within the lower part of the boundary layer  
25 exert large influences on near-surface concentrations of aerosols in the central Arctic.

26 Median daily concentrations were ranging typically between  $15\text{ and }30\text{ cm}^{-3}$  but were a factor  
27 of 3 higher at the ice edge at latitude  $80^\circ\text{ N}$  (days 216-218). At the location of the PI-drift  
28 station on day 244-245 the median concentration was a factor of 100 lower than on days 216-  
29 218, so a temporal change throughout the month of August of this magnitude may be buried  
30 in the noisy data. However, transport time from open water over the pack ice (referred to as  
31 DOI) is shown below to be important and may emphasize the temporal change.

## 1 4.2 CCNC changes with DOI and air mass origin

2 It has become clear from the above discussion that in order to understand the occurrence of  
3 CCNC in the atmosphere over the pack ice an understanding of the synoptic scale systems  
4 advecting heat, moisture, and particles from the surrounding open seas over the pack ice will  
5 be require.

6 Based on the availability of data from key instruments utilized in this study the following  
7 group of the impactor samples were included for further analyses, namely OW-1, MIZ-1, PI-  
8 1, PI-3, PI-6, PI-8, PI-9, PI-10, PI-13 and PI-15. The grey shaded bars in Figure 2 mark the  
9 duration of their respective sampling period. Table 2 gives more information on start – stop  
10 times and sample duration. The observed CCNC were averaged over the impactor sampling  
11 times and Table 2 tabulates the 25<sup>th</sup>, 50<sup>th</sup> (median) and 75<sup>th</sup> percentile CCNC separately for  
12 open water (OW-1), marginal ice zone (MIZ-1) and pack ice (PI-1, 3, 6, 8, 9, 10, 13, and 15)  
13 measurements at ca. 0.2 % SS (counter 1). During sample PI-1 and PI-10 we encountered  
14 episodes of pollution (cf. Fig. 2) during which all pumps automatically were closed. During  
15 the episodes the temporal records of the TDMPS observations seemed unchanged relative to  
16 before its start. We therefore will assume no systematic biases in the calculated median  
17 CCNC and that the chemical composition of the impactors is sufficiently compatible.

18 The backward trajectories shown in Fig. 3, were subjectively classified in four clusters  
19 depending on their geographical origin only. They were calculated for a receptor point of 100  
20 m at the location of the ship. This allowed for an identification of impactor samples  
21 representing similar source regions. The origin of the air during both the 1<sup>st</sup> (PI-1 and PI-6)  
22 and 2<sup>nd</sup> (PI-3, PI-9 and PI-10) clusters was highly variable on a daily basis as of the very  
23 synoptically active period during the first half of the expedition (Tjernström et al., 2012). The  
24 air trajectories of cluster 1 (Fig. 3a) originated easterly from the Barents and Kara Seas. For  
25 cluster 2 (Fig. 3b), they came from the Fram Strait - Greenland Sea area. In both clusters the  
26 air spent a relatively short time over the ice (DOI ~ 2) since last contact with open sea. The  
27 period of trajectory cluster 1 (PI-1 and PI-6) and part of cluster 2 (PI-3) had numerous melt  
28 ponds on the ice surface, with temperatures around 0 °C. The ice-melt was followed by a  
29 drop in temperature to -6 °C for about 2.5 days and included the 3<sup>rd</sup> trajectory cluster (PI-8).  
30 The air origin during the 3<sup>rd</sup> cluster was mainly from Greenland (Fig. 3c). The vertical  
31 component of the air trajectories (not presented) shows a subsiding pathway from the free  
32 troposphere across Greenland to the surface, which suggests that the air sampled onboard

1 *Oden* was of free tropospheric origin. No DOI could be calculated since the trajectories did  
2 not have any contact with the open sea. After this brief snap shot of cold air near-surface  
3 temperatures became semi stationary around -2 °C and hosted part of the 2<sup>nd</sup> trajectory cluster  
4 (PI-9 and PI-10). During the 4<sup>th</sup> (PI-13) and 5<sup>th</sup> (PI-15) clusters, Figs. 3d,e, the air flow was  
5 largely from north western circumpolar over the pack ice for approximately DOI = 8 and from  
6 the direction of the Laptev and East Siberian Seas towards the end of the period but still with  
7 no close contact with open sea. The conditions during the 4<sup>th</sup> trajectory cluster were governed  
8 by a persistent stratocumulus layer that contributed to maintain the temperatures between -2  
9 to -3 °C. The 5<sup>th</sup> trajectory cluster started on 31 August (DOY 244) and ended on September 2  
10 (DOY 246) as the persistent stratocumulus layer went away and the clouds, if present, became  
11 optically thin (Mauritsen et al., 2010), which resulted a drastic drop in temperature to -12 °C  
12 and sunny conditions. During OW-1 (DOY 216-217) we experienced air predominantly from  
13 the ice-covered archipelago north of Canada and Alaska, without any contact with the open  
14 sea within 10 days. Therefore also in this case no DOI could be calculated. During MIZ-1  
15 (DOY 217-218) the air crossed over open water along the east coast of Greenland prior to  
16 sampling at the location of the ship. Trajectories for either OW-1 or MIZ-1 are not presented.

17 Figure 4 translates the time series of Figure 2 and Table 2 into CCNC as a function of the  
18 synoptic scale systems since their last contact with open sea, defined as DOI. Perhaps the  
19 most important result contained in Figure 4 is the loss of CCN approaching a factor of 3  
20 during about the first two days of transport from the ice edge, followed by a recovery.  
21 Herman and Goody (1976) have modeled the formation of fog and cloud in warm moist air  
22 during advection over the pack ice. They concluded that advection fog formed on the first and  
23 second day over the pack ice but lifted to form low stratus on day 3. Losses of CCN to the  
24 surface in the surface mixed layer will therefore be expected to be at a maximum on the first  
25 and second day when drizzle and fallout of fog drops aid deposition to the surface, consistent  
26 with the steep decline seen in Figure 4 and with previous reported studies in the same area  
27 and season (Bigg and Leck, 2001a). Thereafter losses should have continued by wet  
28 deposition at a lower rate, but we actually see an increase in number of CCN in two of the  
29 three impactor samples (PI-6 and PI-13, Table 2) for DOI >4. This feature is again consistent  
30 with previous work by Bigg and Leck (2001a) and indicative of a source of CCN particles in  
31 the inner Arctic.

1 One other much less frequently occurring (a few days out of 40 days expedition in total)  
2 possible cause of the CCNC increase, represented by sample PI-13 (DOI=6.1, Table 2), is  
3 coinciding with a re-coupling and turbulent mixing between a shallow (~150 m deep) surface  
4 based mixed-layer and with a separate mixed-layer located in the upper part of the boundary  
5 layer, which contained stratocumulus clouds (More details in Shupe et al., 2013). The  
6 backward trajectory analysis suggests that the air in the upper boundary layer had come from  
7 the Canadian archipelago (not shown) while that in the lowest 100 m (shown in Fig. 3d) had  
8 been over the ice for at least 10 days. Based on the CCN fingerprint we therefore speculate  
9 that the surface air that mixed with the upper part of the boundary layer was influenced by  
10 continental sources. Several studies from ASCOS support this finding (Paatero et al., 2009;  
11 Chang et al., 2011; Leck et al., 2013; Kupiszewski et al., 2013; Sierau et al., 2014).

12 The extremely low CCNC (median levels of  $1 \text{ cm}^{-3}$ , about 200 nm in diameter for a water  
13 vapor SS at 0.2%) observed during PI-15 (DOI=9.3, Table 2) is related to the meteorological  
14 conditions (Fig. 3e) and aerosol stratification prevailing during the time of sampling of PI-15.  
15 Based on the helicopter profiles observed during ASCOS, Kupiszewski et al. (2013) report on  
16 concentrations of aerosol particles of ca 300 nm in diameter, being very low ( $0.5 \text{ cm}^{-3}$ ) within  
17 the lowermost few hundred meters. Starting on the second half of 31 August the TDMPS  
18 measurements onboard *Oden* also showed a strong decrease in accumulation mode particle  
19 concentration to below  $1 \text{ cm}^{-3}$ . The low aerosol particle concentrations were accompanied by  
20 an almost complete disappearance of clouds, which was observed from ca. 20:00 UTC on 31  
21 August. Mauritsen et al. (2011) hypothesize that the cause of the tenuous cloud regime is that  
22 when the CCNC fall below some critical value, droplets grow large and rapidly sediment out.  
23 This contributes both to keeping the CCNC low, by the removal of the CCN, and to remove  
24 cloud water, thus keeping the clouds optically thin. An analysis of corresponding CCN data  
25 from the previous three *Oden*-based expeditions (Mauritsen et al., 2011) showed that this kind  
26 of tenuous cloud regime occurred about 25% of the time.

27

## 28 **5 The sensitivity of CCNC as a function of water vapor supersaturations**

### 29 **5.1 Measured CCNC as a function of water vapor supersaturations**

30 Figure 5 displays the sensitivity of measured CCNC (averaged over the duration of each of  
31 the impactor samples) as a function of the five levels of water vapor SS between 0.1 and 0.8



1 % seen by the second CCN counter. Increasing the water vapor SS from 0.1 to 0.2% resulted  
2 in a significant increase in CCNC for all impactor samples, but further SS increases resulted  
3 in small or non-existent change in CCNC for samples PI-1, PI-3, PI-6, PI-9, PI-10 and PI-13,  
4 respectively. This feature was also seen in Sample PI-15 but at a much lower absolute level.

5 Figure 6 displays the variation in CCNC with increasing water vapor SS normalized to the  
6 average values for the duration of each of the impactor samples. The similarity in the shape of  
7 CCNC as a function of SS is seen for the PI-1, PI-3, PI-6, PI-9, PI-10, PI-13 and PI-15  
8 impactor samples (Fig. 6 lower panel). It should be noted that the temporal variability in  
9 CCNC covered by each of the impactors is high (Fig. 2 and Table 2) and since the  
10 measurements for each SS only cover about 20% of the time within the start and stop times of  
11 the impactors systematic biases could result. However, since all the seven samples are  
12 showing similar features there is no evident reason to suspect systematic biases. The OW-1  
13 and PI-8 samples, pictured in Fig. 6 (upper panel), show on the other hand a more or less  
14 continuous increase in CCNC with increasing water vapor SS. A similar but weaker  
15 continuous increase in CCNC with increasing water SS was also shown for sample MIZ-1  
16 plotted in Fig. 6 (upper panel).

17 In view of the observed sensitivity of measured CCNC as a function of water vapor SS the  
18 characteristics of the impactor samples could be summarized as follows: i) OW-1 and MIZ-1  
19 with more or less continuously increase in CCNC:s with increasing water vapor SS. The air  
20 origin was predominantly from the ice covered archipelago north of Canada and Alaska and  
21 from over open water along the east coast of Greenland, ii) pack ice sample PI-8 with a similar  
22 feature as of i). Sample PI-8 collected air with possible free tropospheric origin (cluster 3: Fig  
23 3c), iii) samples PI-1, PI-3, PI-6, PI-9, PI-10, PI-13 and PI-15 which all showed a small or  
24 non-existent continuous change in CCNC with increasing water vapor SS > 0.2%. One  
25 common feature for five out of the seven impactor samples was that the sampled air spent a  
26 relatively short time over the ice (DOI ~ 2) since last contact with open sea. The origin of the  
27 air during PI-1 and PI-6 (trajectory cluster 1: Fig. 3a) and PI-3, PI-9 and PI-10 (cluster 2: Fig.  
28 3b) were easterly from the Barents and Kara Seas and from the Fram Strait - Greenland Sea  
29 area. For the remaining two samples PI-13 (cluster 4: Fig. 3d) and PI-15 (cluster 5: Fig. 3e),  
30 the air was advected over the pack ice for more than 6 days since contact with open sea.

1 At first sight the above results suggested that either differences in time of advection of the air  
2 over the pack ice or possible impact from non marine aerosol sources, as in PI-8, did have any  
3 systematic affect on the sensitivity of observed CCNC as a function of water vapor SS.

4 To further search for a relationship between the properties of the summer high Arctic aerosol  
5 and its ability to form CCN, we will use observed aerosol number size distribution data,  
6 additional hygroscopic growth information, and determined aerosol bulk chemistry resolved  
7 over size. We will focus mainly on five samples as representatives for the features  
8 summarized above: MIZ-1, PI-1 (trajectory cluster 1), PI-8 (trajectory cluster 3), PI-10  
9 (trajectory cluster 2) and PI-15 (trajectory cluster 5).

## 10 5.2 $\kappa$ -Köhler theory predictions

11 We next derived aerosol activation-limited-dry-diameter from the measured CCN number  
12 concentrations and TDMPS size distributions by only assuming that larger particles will  
13 activate at lower water vapour SS than smaller. The derived diameters were compared to  $\kappa$ -  
14 Köhler theory (Petters and Kreidenweis, 2007) using a range of  $\kappa$ -values and  $\sigma_{s/a}$ , assuming a  
15 size-independent aerosol chemical composition. Assumed  $\kappa$ -values ranged from 0.1 to 1.  
16 Based on the determined chemical composition of the impactor samples  $\kappa$ -values below 0.1  
17 were not included in the comparison. The aerosol surface tension was also assumed to be size-  
18 independent and equal either to that of pure water ( $\sigma_{s/a}=73 \text{ mN m}^{-1}$  at  $20^\circ\text{C}$ ) or to a value of  
19  $\sigma_{s/a}=50 \text{ mN m}^{-1}$  representing a case of moderate particle surface activity.

20 Figure 7 shows that the aerosol activation-limit-dry-diameter of the samples generally tended  
21 to be larger than the expected diameters from the assumed pairs of  $\kappa$ -and  $\sigma_{s/a}$ . At lower water  
22 vapor SSc and in general for impactor samples MIZ-1, PI-1 and PI-8, the mismatch was less  
23 severe. The predictions showed clearly that impactor PI-10 and PI-15 deviate the most from  
24 the  $\kappa$ -Köhler theory, with a shown increase of the hydrophobic character in the activated  
25 particles with decreasing diameter, with impeded water uptake as a consequence.

26 To further study which aerosol properties that possibly could suppress cloud droplet  
27 formation with decreasing diameter, we will continue to simulate cloud nucleation assuming  
28 Köhler theory. The Köhler theory will be combined with a Lagrangian adiabatic air parcel  
29 model that solves the kinetic formulation for condensation of water on size resolved aerosol  
30 particles. For details on the approach we refer to the Supplementary material. In section 8 the

1 CCNC simulations will use the observed aerosol number size distribution data and  
2 assumptions on the composition on the inorganic/organic aerosol system resolved over size.  
3 In the later case the water-soluble determined impactor data will be used together with a best  
4 guess of the properties of the “missing non water-soluble fraction”, that is the fraction of  
5 particles not classified by the chemical determinations. Before presenting the results from the  
6 CCNC simulations in section 8, sections 6 and 7 will discuss how to assume the “missing  
7 non-water soluble” aerosol fraction using a comparison between the TDMPS number size  
8 distribution and the converted total water-soluble mass determined by the impactors.

## 10 **6 Size resolved aerosol water soluble chemical composition by number**

11 Figure 8 displays a comparison between the converted total water-soluble mass determined by  
12 the impactors and the TDMPS number size distribution. Figure 9 gives additional details on  
13 the ionic contribution of  $\text{Ca}^{2+}$ ,  $\text{Na}^+$ ,  $\text{Cl}^-$ ,  $\text{SO}_4^{2-}$  and MSA to the total water-soluble mass  
14 determined.

15 *Impactor sample PI-10:* The average number size distribution collected during impactor  
16 sample PI-10 showed a strong bimodal distribution (Fig. 8, PI-10), with the Aitken and  
17 accumulation modes possibly separated by a Hoppel minimum (Hoppel et al., 1994). This is a  
18 known characteristic of an aerosol population modified by cloud/fog processing (Hoppel et  
19 al., 1986) and originating over a marine area (Heintzenberg et al., 2004). That the air  
20 trajectory-cluster (Fig. 3b) originated predominantly from the MIZ of the Fram Strait -  
21 Greenland Sea area in foggy conditions provides a coherent picture.

22 Guided by previous findings from past *Oden*-expeditions (Karl et al., 2012; Kerminen and  
23 Leck, 2001; Leck and Bigg, 2005b; Leck and Persson, 1996; Leck et al., 2002) we suggest  
24 that the pronounced accumulation mode in part resulted from condensational growth on pre-  
25 existing Aitken mode particles from precursor gases such as the DMS oxidation products with  
26 subsequent activation as cloud droplets. Activated particles could then have grown via in-  
27 cloud aqueous phase oxidation of gases such as sulfur dioxide ( $\text{SO}_2$ ), resulting in release of  
28 larger particles following droplet evaporation (Lelieveld and Heintzenberg, 1992). Figure 9  
29 (PI-10) confirms the expected large fraction of the oxidation products of DMS ( $\text{SO}_4^{2-}$  and  
30 MSA) to total analyzed water-soluble constituents in the accumulation mode. When the air  
31 has been in very recent contact with the MIZ/open water (DOI=1.4, Table 2), a further

1 mechanism would have involved the release of accumulation mode primary marine particles  
2 (sea salt and biogenic) from the MIZ via bubble bursting (Nilsson et al., 2001; Leck et al.,  
3 2002; Bigg and Leck, 2008). The sea salt contribution to the accumulation mode of the PI-10  
4 water-soluble aerosol fraction is shown in Fig. 9 (PI-10).

5 **Impactor samples MIZ-1 and PI-1:** A similar strong bimodal distribution with the Aitken  
6 and accumulation modes separated with a Hoppel minimum was seen in samples MIZ-1 and  
7 PI-1 (Fig. 8, MIZ-1; PI-1). Their accumulation modes were however less developed relative  
8 to the Aitken mode compared to sample PI-10, which would suggest an aerosol to a lesser  
9 extent modified by in cloud processing via in-cloud aqueous phase oxidation of SO<sub>2</sub>. Fig. 9  
10 (MIZ-1) shows that sea salt from bursting bubbles at the sea-air interface also contributed to  
11 the water-soluble fraction in the Aitken and -accumulation mode. In a parallel study during  
12 ASCOS by Leck et al., 2013 (Fig 4 middle panel) the additional contribution of particulate  
13 polysaccharides (building blocks of <sup>4</sup>polymer gels) from the same bubble bursting mechanism  
14 can be seen<sup>5</sup>. The dominance of Ca<sup>2+</sup> for sub-accumulation mode particle seen in Fig. 9 (PI-1)  
15 indirectly suggests the presence of polysaccharide molecules inter-bridged with divalent ions.  
16 A domination of Ca<sup>2+</sup> for smaller particles was also observed in samples PI-10 and PI-15.

17 **Impactor sample PI-15:** The impactor sample PI-15 shared the bimodal characteristics of  
18 samples PI-10, PI-1 and MIZ-1, but at a much lower absolute number concentration and with  
19 a wider minimum between the accumulation mode and a sub-Aitken mode, see Fig. 8 (PI-15).  
20 The extremely low CCNC observed during PI-15 was discussed in section 3.2 to be related to  
21 the prevailing meteorological conditions (Fig. 3e) and aerosol stratification (Kupiszewski et  
22 al., 2013). Below 10 nm (not shown in Fig. 8, PI-15) a strong mode of recent nucleated  
23 particles was observed. In addition, the measurements showed that the availability of  
24 condensable vapors was limited in the boundary layer during PI-15, and that the concentration  
25 of DMS (below 4 ppt (v)), a precursor to sulfuric acid, was not sufficient to sustain growth

---

<sup>4</sup> Marine gels or polymer gels are produced by phytoplankton and biological secretions of sea ice algae at the sea-air interface. The polymer gels are made up of water-insoluble, heat resistant, highly surface-active and highly hydrated (99% water) polysaccharide molecules spontaneously forming 3-dimensional networks inter-bridged with divalent ions (Ca<sup>2+</sup>/Mg<sup>2+</sup>), to which other organic compounds, such as proteins and lipids, are readily bound (Verdugo, 2012 gives a review).

<sup>5</sup> The limited mass collected by the highly size resolved LPI impactors did not allow for the analyses of polysaccharides.

1 into the super 10 nm diameter size range. This also left unexplained the observed co-  
2 appearance of particles in the 20–50 nm diameter size range coinciding with the nucleation.  
3 To explain the nucleation event Karl et al. (2013) suggested a novel route to atmospheric  
4 particle generation that appears to be operative during PI-15. It involves the fragmentation of  
5 primary marine polymer gels into the air from evaporating fog and cloud droplets. The ionic  
6 composition of the sub-accumulation mode of sample PI-15 was shown negligible in not only  
7 the sulfur containing but all other water-soluble constituents but for  $\text{Ca}^{2+}$  (Fig. 9, PI-15). This  
8 observation supports the findings by Orellana et al. (2011) and Leck et al. (2013) who  
9 observed polymer gels in atmospheric samples during the course of PI-15. Sulfur components  
10 and  $\text{Ca}^{2+}$  dominated the accumulation mode. In view of above discussion polymer gels could  
11 potentially have contributed to the missing non water-soluble fraction not only in PI-15 but  
12 also in samples MIZ-1, PI-1 and PI-10.

13 **Impactor sample PI-8:** The single Aitken mode distribution of PI-8, peaking at 45 nm  
14 diameter (Fig. 8, PI-8), suggests an aerosol population sourced in the free troposphere (Leck  
15 and Persson, 1996). The air trajectory in Fig. 3c showing a subsiding pathway from the free  
16 troposphere via across Greenland to the surface also points to air of free tropospheric origin.  
17 The low marine biogenic factor calculated for ASCOS by Chang et al. (2011) again  
18 consistently suggests air arriving at the surface without recent contact with the marine  
19 influenced boundary layer. Note the high contribution of  $\text{Na}^+$  and  $\text{Cl}^-$  and  $\text{Ca}^{2+}$ . This likely  
20 free tropospheric origin of PI-8 limits our knowledge of possible aerosol sources and thus for  
21 candidates of the missing non water-soluble fraction seen in Fig. 8 (PI-8).

22

## 23 **7 Assuming the missing non-water soluble aerosol fraction**

24 Guided by the size resolved bulk chemical information given in Figure 9 and bulk chemical  
25 and electron microscope analyses resulted not only from ASCOS (Chang et al., 2011;  
26 Hamacher-Barth et al., 2013; Karl et al., 2013; Leck et al., 2013; Orellana et al., 2011) but  
27 from all three previous expeditions in the summers of 1991, 1996 and 2001 (Bigg and Leck,  
28 2001a,b; 2008; Leck and Persson, 1996; Leck and Bigg, 1999; 2002; 2005a,b; 2010; Leck et  
29 al., 2002; Lohman and Leck, 2005) we will assume the sub-Aitken mode particles (Fig. 10a-c)  
30 to be made up of externally mixed organically derived small polymer gels with hydrophobic  
31 and hydrophilic properties to a various degree (Xin et al., 2013; Orellana et al., 2011).  
32 Statistical analysis of the aerosol size distribution data collected over the inner Arctic

1 recorded in the years 1991, 1996, 2001, and 2008 classified 17% of the observed time period  
2 to be characterized by the spontaneous appearance of several distinct size bands below 50 nm  
3 diameter as discussed in Karl et al. (2013). However there appears to be an inconsistency  
4 when comparing observations of small particle formation over the inner Arctic and those  
5 south of the pack ice area. The studies at Alert, Canada (82,5°N: 62,3°W) and NyÅlesund,  
6 Svalbard (79°N: 11,9°E) in spring and early summer by Engvall et al., (2008) and Leaitch et  
7 al. (2013) showed nucleation events followed by subsequent growth, which could be  
8 explained by solar radiation in concert with the presences of precursor gases and attendant  
9 low condensational sinks. Possible reasons for the inconsistency could be that the DMS  
10 source and photochemical sink generating the precursor gases for nucleation and early growth  
11 is both seasonal and temperature dependent (Leck and Persson, 1996a,b; Kerminen and Leck,  
12 2001; Karl et al., 2007; 2012). Given that, perhaps the main difference between the studies  
13 concerns how efficiently nucleation and growth of particles resulting from DMS oxidation are  
14 predicted by the choice of model and lack of observations to constrain the assumptions made.

15 As the sub-Aitken particles grow, we will assume the particles resulting from deposition of  
16 acids/organic vapors on a polymer gel-aggregate (Fig. 10d-e) or typical of a sulfur-containing  
17 particle with hygroscopic properties in which any nucleus has become obscured by the  
18 surrounding of a sulfate-methane sulfonate-ammonium complex (Fig. 10f). The Aitken mode  
19 and smaller accumulation mode below ca 100 nm in diameter will be assumed to be  
20 represented by external mixtures of gels and internally mixed sulfur constituents (Fig. 10g),  
21 whereas accumulation mode particles at a few hundred nanometers diameter will be assumed  
22 to be internal mixtures of gels and sulfur constituents.

23 Finally, the upper end of the accumulation mode above 200 nm in diameter will be assumed  
24 to be composed of internal mixtures resulting from multiple sources, as in Figure 10h,  
25 showing sea salt and a bacterium coated with an organic film and by the concentric rings  
26 typical of droplets of sulfuric acid. In addition, film drops could add gel material with salt-  
27 free water with or without any attached microorganism, Fig. 10i shows an example of the  
28 latter. In Bigg and Leck (2008) it was suggested that the highly surface-active polymer gels  
29 could attach readily to the surface of rising bubbles and self-collide to form larger aggregates.  
30 Consequently, polymer gels and their aggregate production, as well as the embedded solid  
31 particles such as bacteria, phytoplankton and its detritus, can be carried selectively to the  
32 surface microlayer by rising bubbles. Before bursting, bubbles stay in the microlayer for some

1 time and therefore are likely to acquire walls, consisting to a large extent of strengthening  
2 gels, with embedded particulate matter that may be points of weakness as the water drains  
3 from between the walls. Following the burst, the film drop fragments would not be drops of  
4 salt water but of gel material with salt free water and any particles attached to the fragments.  
5 Previous reported result of individual particles by Bigg and Leck (2001, 2008), Leck et al.  
6 (2002), and Leck and Bigg (2005a, b, 2010) collected over the pack ice have failed to find  
7 evidence of sea salt particles of less than 200 nm in diameter. The presence of bubbles  
8 observed in the water column (Norris et al., 2011) provides a plausible mechanism for getting  
9 surface material airborne. In all this supports the suggested mechanism for getting the primary  
10 biogenic material at the open-lead<sup>6</sup> surface airborne. Even though jet drop particles (“jet  
11 drops”: centered around 1  $\mu\text{m}$  diameter) are mainly composed of sea salt, they have been  
12 observed over the Arctic pack ice area to be partly coated by polymer gels (Leck et al., 2002).  
13 An example is seen in Fig. 10h.

14 For each of the impactor samples the “missing non water-soluble fraction” not classified by  
15 the chemical determinations is listed in Table 2, being on average 54%. The fractions were  
16 derived from the difference between the observed total particle concentration seen by the  
17 TDMPS and the estimated total number concentration based on the chemical determinations.

18 As a surrogate for the unexplained fraction assumed to be organic (gels and condensed  
19 organic vapors) in nature we will use slightly water-soluble and non water-soluble proxy  
20 constituents. As a slightly water-soluble but moderately surface-active dicarboxylic acid we  
21 used adipic acid, which has been observed in ambient particulate matter including in the  
22 Arctic (Narukawa et al., 2002). Also detected in Arctic aerosol particles (Fu et al., 2009) was  
23 cis-pinonic acid, which was chosen as a surrogate for highly surface-active properties of the  
24 missing fraction with insignificant lowering of the water activity. Predicting a surface tension  
25 of mixtures of ionic solutions with surface-active organics is an ambiguous task. Inorganic  
26 components may either enhance or inhibit the surface tension depression caused by  
27 surfactants, depending on both concentration and substance (Tuckermann, 2007). Hence, one  
28 single best scheme to predict surface tension of mixed aqueous solutions is not likely to exist.  
29 In this study we set the aerosol surface tension for adipic acid to  $\sigma_{s/a}=68 \text{ mN m}^{-1}$  (Lohmann

---

<sup>6</sup> The high Arctic open leads can be described as ever-changing open water channels comprising 10-30% of the ice pack ice area, ranging from a few meters up to a few kilometers in width.

1 and Leck, 2005) and use a value of  $\sigma_{s/a}=38 \text{ mN m}^{-1}$  in the case of cis-pinonic (Tuckermann,  
2 2007). The surface tension of the internally mixed accumulation mode aerosol was obtained  
3 by weighting the surface tension of each soluble constituent by its mass fraction.

4 Table 3, lists the various assumptions concerning the “missing non water-soluble fraction”  
5 used in the modeling, idealized for one size bin of a wet aerosol. The wet aerosol is in general  
6 assumed to consist of three more or less non-water-soluble units with known determined  
7 water-soluble constituents and 1/3 of dry mass not being determined. Diamonds inside the  
8 droplets indicate a water-insoluble particle fraction. The color scale of the droplet bulks (from  
9 gray to blue) show increasing ionic concentration, equivalent to a lowering of water activity.  
10 Orange and red droplet fringes show various degrees of depressions in surface tension, red  
11 being the strongest.

12 For the INSOL simulation the missing fraction is assumed to be either a completely water-  
13 insoluble core (Fig 10d,h: gel or a bacterium) within the water soluble droplet or a sulfur-  
14 containing particle in which any gel-nucleus has become obscured by the surrounding of a  
15 sulfate-methane sulfonate-ammonium complex (Fig. 10f) was captured.

16 In the AD (low water-solubility and moderate surface active) and PIN (low water-solubility  
17 and highly surface active) cases, particles are resulting from deposition of organic vapors on a  
18 polymer gel particles. Fig. 10e shows an example.

19 When the externally non-water soluble fraction was assumed to be made up by pure adipic  
20 and/or cis-pinonic acid (AD\_ext and PIN\_ext respectively) it mimics the behavior of a  
21 polymer gel (Figure 10b-c; upper left of Fig. 10g: Fig 10j): with shown interaction of its  
22 hydrophilic and hydrophobic entities (Orellana et al., 2001; Xin et al., 2013). The proportion  
23 between AD\_ext and PIN\_ext was linearly combined, assuming for example a 50/50 adipic/cis-  
24 pinonic acid external particle mixture.

25 The SOL assumption only takes the chemically determined water-soluble aerosol fraction into  
26 account. This then represents an externally mixed aerosol with the water-soluble, detected  
27 compounds as one part (2/3) and a completely CCN-inactive part (1/3) as the other (Fig 10a).

28



## 1    **8 Predicting CCNC**

2    In the following section, we will present and discuss the results from the simulations in the  
3    order of PI-1, PI-8, PI-10, PI-15 and MIZ-1. Figure 11 is a compilation of all simulations.  
4    First to be noted is that the modeling results in the PIN case, where the missing fraction was  
5    assumed to behave like an internally mixed cis-pinonic acid; low water-solubility and highly  
6    surface active, consistently over-predicted the observed CCNC for all five impactor samples.  
7    These runs are therefore excluded in the graphs of Fig. 11.

8    **Impactor sample PI-1:** According to the aerosol activation-limit-dry-diameters shown in Fig.  
9    7, the scans at the three lowest water vapor SS (0.10, 0.15, 0.20 %) activated particles within  
10    the accumulation mode. For the two highest levels of water vapor SS (0.37 and 0.62%),  
11    particles within the Hoppel minimum down to ca. 60 nm in diameter were activated (Fig. 8,  
12    PI-1).

13    As shown in Fig. 11 (PI-1) the simulation runs including the SOL, AD\_ext and PIN\_ext  
14    assumptions of the non-water soluble missing fraction were all able to capture the observed  
15    CCNC within one standard deviation ranging from 0.10% to 0.62% water vapor SS. The  
16    shown activation for particles with decreasing diameter argues for a relatively increased  
17    influence of external mixtures of Fig 10 a-c type particles at the large-end tail of the Aitken  
18    mode. Also the case AD and INSOL did in general capture the observed CCNC but over  
19    predicted the CCNC for the highest level of SS. Hence, the aerosol in the accumulation size  
20    range was suggested to be mixtures of the type of particles exemplified in Fig 10g-i but  
21    possibly also of type 10d-f.

22    **Impactor sample PI-10:** Based on the aerosol activation-limit-dry-diameters for PI-10 (Fig.  
23    7) the scanning, with all five water vapor SS (0.10, 0.15, 0.20, 0.41 and 0,73 %) included,  
24    activated the accumulation mode particles down to ca. 80 nm diameter.

25    Similar to PI-1 all assumptions of the non-water soluble missing fraction were able to  
26    reproduce the observed CCNC within one standard deviation below 0.20% water vapor SS  
27    (Fig 11, PI-10). However all calculations above 0.20% SS over-predicted the observed  
28    CCNC. This result indicates that neither using the most conservative assumption on the  
29    missing fraction (INSOL: internal mixture with a completely insoluble and non-surface active  
30    core) nor using the assumption of an externally mixed aerosol with 2/3 being water-soluble

1 and 1/3 being completely CCN-inactive could predict the sensitivity of the observed CCNC as  
2 a function of water vapor SS.

3 **Impactor sample PI-15:** For particle sizes above 10 nm in diameter, PI-15 shared the bimodal  
4 characteristics with samples PI-1 and PI-10, but with a wider minimum between the  
5 accumulation mode and a sub- Aitken mode (Fig. 8, PI-15). As the extremely low, (usually  
6 below  $0.5 \text{ cm}^{-3}$ ), aerosol particle concentrations resulted in an almost complete disappearance  
7 of low clouds (Mauritsen et al., 2011) and clear sky's during the duration of PI-15 the  
8 minimum is primarily not a result of an aerosol population modified by in cloud/fog  
9 processing (Hoppel et al., 1986). Instead the results by Gao et al. (2012), Leck et al. (2013)  
10 and Orellana et al. (2011) suggests that the accumulation mode instead was maintained by gel  
11 particles sourced from the open-lead surface microlayer.

12 Based on the aerosol activation-limit-dry-diameters for PI-15 (Fig. 7) the CCN-counter  
13 activated particles within the accumulation mode between 130 to 200 nm in diameter. The  
14 simulations in Figure 11 (PI-15) showed that the SOL and AD\_ext assumptions gave the best  
15 over-all fit to the observed CCNC. It can be argued that the activated fractions of the  
16 accumulation mode encompassed an external mixture of particles with internal mixtures of  
17 water-soluble constituents strong in DMS- derived sulfur and particles entirely CCN-inactive.  
18 An alternative explanation could be that the water uptake was impeded and perhaps requires  
19 longer than 50 sec wetting/growth time in the CCN-counter. The latter property is consistent  
20 with the shown increase of the hydrophobic character in the activated particles with  
21 decreasing diameter seen in Fig 7 (PI-15). In agreement with the observed and modeled  
22 chemical behavior of the high Arctic polymer gels with their hydrophilic and hydrophobic  
23 segments (Orellana et al. 2011; Xin et al. (2013), water vapor does not uniformly condense on  
24 the gel since only part of the surface exhibits strong hydrophilicity. Thus as discussed above  
25 the polymer gels would be expected to show initially only partial wetting character below  
26 100% RH but given enough time a high CCN activation efficiency, which is promoted by its  
27 surface-active properties (cf. the PIN\_ext case in Fig. 11, PI-15) of the gels (Ovadnevaite et  
28 al., 2011).

29 **Impactor sample PI-8:** As identified above, sample PI-8 was the only sample out of all  
30 samples collected in the pack ice with a more or less continuous increases in CCNC with  
31 increasing water vapor SS. PI-8 also differed from the above sample in its single Aitken

1 modal number distribution peaking at 45 nm in diameter with a tail into the accumulation  
2 mode (Fig.8, PI-8) causally related to its source in the free troposphere with likely marginal  
3 influence from marine sources. Ranging from 0.10 to 0.73% water vapor SS particles between  
4 50 to 170 nm in diameter were activated (Fig. 7).

5 As shown in Figure 11(PI-8), the SOL and AD\_ext and PIN\_ext assumptions gave the best  
6 over-all fit to the observed CCNC but only the PIN\_ext case was able to reproduce the  
7 measured CCNC within one standard deviation for the whole supersaturation range. It can be  
8 argued that the activated fractions of the broad Aitken mode encompassed an external mixture  
9 of particles with low water-solubility that are highly surface-active and internal mixtures of  
10 water-soluble constituents.

11 **Impactor sample MIZ-1:** Impactor sample MIZ-1 showed similar to the samples PI-1, PI-10  
12 and PI-15 a bimodal aerosol number distribution with the Aitken and accumulation modes  
13 separated with a Hoppel minimum (Fig. 8, MIZ-1) but exhibited similar to PI-8 a more or less  
14 continuous increases in CCNC with increasing water vapor SS.

15 Based on the aerosol-activation-limit-dry-diameters for MIZ-1 (Fig. 7) the range of all five  
16 water vapor SS (0.1 to 0,8 %) activated the particles in both the accumulation – and Aitken  
17 mode down to ca. 50 nm in diameter.

18 As seen in Figure 11(MIZ-1), none of the simulated cases was able to reproduce the measured  
19 CCNC (within one standard deviation) over the entire supersaturation range. For the lowest  
20 range of chosen water vapor SS the discrepancy is shown as an under-prediction of the  
21 observed CCNC whereas quite the opposite is seen for SS above 0.2 %.

22

## 23 **9 Modifying the condensation accommodation coefficient**

24 A general conclusion to be drawn from the above simulations is the shown hydrophobic  
25 character of the collected aerosols, which in turn would impede water uptake with decreasing  
26 diameter of the aerosol. This was also indicated in the deviation from  $\kappa$ -theory discussed in  
27 section 5.

28 To further study this “hydrophobic” feature of the high Arctic aerosol we added two  
29 simulations based on the AD simulation but with a modified condensation accommodation  
30 coefficient,  $\alpha_c$ . The condensation accommodation coefficient is a quantity characterizing of

1 the behavior of the water molecules in their collisions with the aerosol surface. The value of  
2  $\alpha_c$  depends on the surface nature and state as well as on the water vapor supersaturation  
3 pressure.

4 It has been proven difficult to determine  $\alpha_c$  experimentally. Davis, 2006 reports on values  
5 varying several orders of magnitude. For pure water and aqueous ionic solutions without  
6 surface covers several recent studies indicate that  $\alpha_c$  is close to 1 (e.g. Winkler et al., 2004,  
7 Winkler et. al., 2006, Morita et al., 2004). However, several additional studies indicate that  
8 water vapor mass transport across the droplet-air interface in atmospheric aerosol may be  
9 limited, consistent with a lower value for  $\alpha_c$  (e.g. Shantz et al., 2010, Ruehl et al., 2008 and  
10 Chuang, 2002). Impeding water vapor mass transfer slows down the kinetics and this could  
11 result in that the aerosol droplets do not have long enough time to grow to cloud droplet sizes  
12 in the CCN counter.

13 Consistent with the ambient measurements laboratory studies by Abbatt et al. (2005) showed  
14 that thick covers of solid stearic acid were able to shut down the CCN ability of ammonium  
15 sulfate particles and the authors attributed this phenomenon to kinetic effects. Takahama and  
16 Russell (2011) found, using molecular dynamics simulations, that  $\alpha_c$  of a partially covered  
17 water surface is roughly proportional to the fractional surface coverage. In this study, we  
18 tested two different surface coverage scenarios referred to as AC1 and AC2. The AC1  
19 scenario had the same properties as the AD case, but with a constantly low  $\alpha_c=10^{-3}$ . This  
20 would correspond to an almost completely covered aerosol droplet with unlimited resources  
21 of surface-covering molecules. AC2 shared the properties with AC1 assumption except that is  
22 was assumed that the available surface covering agent is limited so that the every particle has a  
23 constant absolute surface area covered. This can be expressed by  $\alpha_c=1-(D_0/D)^2$  for  $D>D_0$  and  
24  $\alpha_c=0$  for  $D\leq D_0$ , where  $D$  is the wet particle diameter and  $D_0$  is a reference diameter. This  
25 parameterization makes  $\alpha_c=0$  for small wet diameters and asymptotically approach unity for  
26 large wet diameters. Clearly, there are multiple other choices of parameterizations, which  
27 would serve as well, but the data available is not sufficient to distinguish between them.  
28 Neither is it possible to unambiguously determine a best value for  $D_0$ . Hence, the AC1 and  
29 AC2 simulations should be viewed as tests of the idea that kinetic effects could reduce the  
30 CCN ability as suggested by Abbatt et al. (2005) and Takahama and Russell (2011). Table 4,

1 lists the new assumptions concerning the “missing non water-soluble fraction” used in the  
2 AC1 and AC2 modeling. Black edges indicate surface covers impeding water vapor mass  
3 transport across the surface, yielding a lower condensation accommodation coefficient.

4 The simulation using the AC1 assumption under-predicted the observed CCNC within one  
5 standard deviation for the full range of water vapor SS studied and for all five impactor  
6 samples. These simulations are therefore not included in the compilation of the impactor  
7 samples shown in Fig. 12. The result of the AC2 sceneries will be discussed below.

8 The AC2 simulation of sample PI-1 was able to capture the sensitivity of the measured CCNC  
9 within one standard deviation as a function of all five levels of water vapor SS ranging from  
10 0.1% to 0.6%. This argues for the type 10 d,e particles, with a limited water vapor mass  
11 transport across the droplet-air interface, co-existing with the type 10a-c type of particles at  
12 the large end tail of the Aitken mode. For impactor sample PI-15 the AC2 CCNC simulation  
13 as a function of all five levels of water vapor SS showed similarly successful (Fig. 12, PI-15).

14 In section 8 above it was argued that the activated fractions of the accumulation mode  
15 particles (PI-15) encompassed an external mixture of partly wetted gel-type particles with  
16 their shown hydrophobic character and impendent water vapor uptake (being more dominant  
17 with decreasing diameter) with internal mixtures of water-soluble constituents strong in DMS-  
18 derived sulfur. Also for sample PI-10 (Fig. 11) this feature of a limited water vapor mass  
19 transport across the droplet-air interface of the accumulation mode seems also to be the best  
20 possible explanation of the over-prediction of CCNC seen for water vapor SS above 0.2% for  
21 PI-10.

22 It was argued based on the simulations shown in Fig. 11(PI-8) that the activated fraction of  
23 the Aitken mode of impactor sample PI-8 encompassed an external mixture of particles with  
24 low water-solubility that are highly surface active and with internal mixtures of water-soluble  
25 constituents. The simulations with modified condensation accommodation coefficients  
26 however strongly under-predicted the observed CCNC:s at the higher supersaturations, see  
27 Fig. 12 (PI-8). Therefore, we did not find any evidence for a restricted water uptake in this  
28 sample.

29 The simulations performed for sample MIZ-1 in section 8 were not at all successful in  
30 reproducing the measured CCNC within one standard deviation for the entire supersaturation

1 range (broadly activated particles in both the accumulation – and Aitken mode down to ca. 50  
2 nm in diameter): the lowest range of water vapor SS showed an under-prediction of the  
3 observed CCNC whereas an over-prediction was seen for SS above 0.2 %. With the added  
4 assumption in the AC2 simulation it was still hard to capture the overall continues increase in  
5 observed CCNC with increasing water vapor SS pressures.

6 We note further that by lowering the  $D_0$  in the AC2 simulation (physically that is equivalent  
7 to increasing the available surface coverage area), it seems possible to get a better match. We  
8 do however consider this as curve fitting beyond the scope and data available of this study.

9

## 10 **10 Summary and Conclusions**

11 Concentrations of cloud condensation nuclei were measured throughout an icebreaker  
12 expedition (ASCOS) over the central Arctic Ocean, including a 3-week ice drift operation at  
13 87°N, from August 3 to September 9, 2008. Median daily CCN concentrations were typically  
14 ranging 15 to 30  $\text{cm}^{-3}$ , being a factor of three higher at the MIZ. The most conspicuous feature  
15 of the time series of CCN was the 2-3 orders of magnitude range of concentrations, ranging  
16 from below one to 100  $\text{cm}^{-3}$ . Highest concentrations occurred over the open water just south  
17 of the ice edge in August. Losses of CCN as the air progressed over the pack ice and mixing  
18 processes in an often strongly stratified near-surface layer were suggested to contribute most  
19 strongly to this large range (Bigg et al., 2001). The losses of CCN (measured at 0.2%  
20 supersaturation) approaching a factor of three during the first ca two days in air progressing  
21 from the open sea to the pack ice were not surprising in view of the usual evolution of  
22 cloudiness that accompanies the progression into the pack ice. It was surprising however that  
23 the losses did not continue for longer transport times. A local surface source, presumed to be  
24 the bursting of bubbles on the surface of open leads, was suggested in consistency with other  
25 previous independent analyses (e.g. Leck and Bigg, 2005a). This open lead source of particles  
26 has recently been demonstrated to be biogenic and consist of marine polymer gels (Orellana et  
27 al., 2001; Leck et al., 2012).

28 Previous search for a relationship between the properties of the summer high Arctic aerosol  
29 and its ability to form CCN by assuming equilibrium Köhler theory or conventional  $\kappa$ -Köhler  
30 theory (Zou et al., 2001, Bigg and Leck, 2001a; Martin et al., 2011) the calculations generally  
31 tended to over-predict the observed CCNC. The prediction was about 30-60% higher than the

1 observed ones for water vapor supersaturation above 0.4% (Martin et al., 2011). Below 0.2%  
2 water vapor supersaturation in general an excellent agreement was achieved. Further,  
3 Lohmann and Leck (2005) found it necessary to invoke a highly externally mixed surface-  
4 active Aitken mode in order to explain the observed CCNC over the pack ice.

5 Intrigued by the above results the present study was aimed to further reduce some of the  
6 uncertainties surrounding the CCN properties promoting/suppressing cloud droplet formation  
7 in a marine environment with limited influences from man-made activities. The main  
8 advantage and motivation compared to previous high Arctic CCN-closure studies was the use  
9 of water-soluble aerosol bulk chemistry obtained from highly size resolved impactor samples.  
10 This enabled us also to make a similarly highly size resolved best “guess” of the unexplained  
11 number fraction assumed to be organic in nature. Guided by chemical analyses based on  
12 electron microscope data resulting from all three previous expeditions (Bigg and Leck,  
13 2001a,b; 2008; Leck and Bigg, 1999; 2002; 2005a,b; 2010; Leck et al., 2002; Lohman and  
14 Leck, 2005) we used various water-soluble, slightly water-soluble and non water-soluble  
15 proxy constituents. One further advantage was the possibility to compare the measured and  
16 modeled CCNC for more than one set level of water vapor SS, ranging from 0.1% to 0.8%.  
17 The simulations assumed equilibrium Köhler theory and were based on the diffusional growth  
18 equation. In addition, calculations were performed using  $\kappa$ -Köhler theory.

19 The results of this study are consistent with previous results by Martin et al. (2011) in that  
20 conventional  $\kappa$ -Köhler theory fails to predict the CCNC for samples in air that had been  
21 advected over the pack ice. Simulating the cloud nucleation process using a Lagrangian  
22 adiabatic air parcel model that solves the kinetic formulation for condensation of water on  
23 size resolved aerosol particles at high supersaturation resulted in severe over-predictions of  
24 the CCNC when even the most conservative assumption on the unknown fraction was used. A  
25 general conclusion to be drawn from the CCN simulations and from the calculated deviation  
26 from  $\kappa$ -Köhler theory is an increase of the hydrophobic character in the activated particles  
27 with decreasing diameter. This suggested hydrophobic character of the high Arctic aerosol  
28 was also shown in the study of Martin et al. (2011) and would in turn impede water uptake  
29 with decreasing diameter of the aerosol.

30 We tested whether introducing kinetic limitations on water uptake could explain these aerosol  
31 properties suppressing cloud droplet activation above 0.4% water vapor super saturation. A

1 fixed non-size resolved low water uptake rate consistently produced too low CCNC, but a size  
2 dependent assumptions was in general able to capture the sensitivity of the measured CCNC  
3 within one standard deviation as a function of all the five levels of water vapor SS ranging  
4 from 0.1% to 0.8%.

5 The results further suggested that either differences in time of advection of the air over the  
6 pack ice, where additional primary marine aerosol sources and atmospheric gas-phase and  
7 aerosol dynamical processes could change the properties of the CCN prior to collection, or  
8 possible impact from non natural aerosol sources did have systematic effects on the sensitivity  
9 of observed CCNC as a function of water vapor supersaturation. What seems to be of primary  
10 importance is the size resolved state of mixture together with physical and chemical behavior  
11 of the fraction of the aerosol population that will undergo droplet activation.

12 To explain the results we propose that the portion of the internally/externally mixed water  
13 insoluble particles, which were physically and chemically behaving as polymer gels, was  
14 larger in the corresponding smaller aerosol sizes ranges. The suggestion of the presence of a  
15 non-water soluble organic fraction of the CCN population either promoting/suppressing cloud  
16 droplet formation thus did not deviate from the conclusions drawn by Lohman and Leck  
17 (2005) and Martin et al., (2011). The interaction of the hydrophilic and hydrophobic entities  
18 on the structures of polymer gels during cloud droplet activation strongly suggests a  
19 dichotomous behavior with at first only partial wetting character and only weak hygroscopic  
20 growth. Given time, a high CCN activation efficiency is achieved, which is promoted by the  
21 hydrophilicity or surface-active properties of the gels (Ovadnevaite et al., 2011). The results  
22 of this study argue for the behavior of the high Arctic aerosol in CCN-counters operating at  
23 high relative humidities being not fully explained by conventional Köhler theory where the  
24 only free parameters are hygroscopicity and surface tension. However, we note that particles  
25 with kinetically restricted growth can be activated in real cloud situations even if they are not  
26 counted in the CCN counter. It might be that the time (~50 s) inside the CCN counter is  
27 insufficient for the particles to grow to large enough sizes. The results by Chuang (2003)  
28 show consistency with the findings in this study in that he found that an eternally mixed  
29 fraction of ambient aerosol, with very slow water uptake, could account for some  
30 observations of particle water uptake that could not be explained with conventional Köhler  
31 theory.



1 Clearly, there still remain many uncertainties in the evolution of cloud-active particles in the  
2 high Arctic and probably elsewhere. One evident outcome from this study is that we have to  
3 stop regarding the cloud active particles over remote marine areas to be simply inorganic  
4 soluble salts to in addition consist of internal/external mixtures of soluble or slightly soluble  
5 organics, which likely will influence the equilibrium water vapor pressure and decrease  
6 surface tension of the droplets to be formed. This study also suggests that the Köhler equation  
7 used for simulating cloud droplet activation is not sufficient for describing the condensational  
8 growth during of the interaction of the hydrophilic and hydrophobic entities on the structures  
9 as of the polymer gels suggested to be present at the MIZ and over the pack ice area. Different  
10 approaches are suggested as revisions of Köhler theory, one being to utilize a larger number  
11 of size resolved observations of morphology, state of mixture and chemical and physical  
12 behavior of individual cloud-active particles.

13

14

## 15 **Acknowledgements**

16 We greatly thank Maria Martin, Staffan Sjöberg, Douglas Orsini, Berko Sierau, Ulrike  
17 Lohmann, Erik Swietlicki and Jost Heintzenberg for the CCN and aerosol physical data  
18 collection and quality assurance work. Jost Heintzenbergs's comments on an the article are  
19 appreciated. This work is part of ASCOS (the Arctic Summer Cloud Ocean Study). ASCOS  
20 was made possible by funding from the Knut and Alice Wallenberg Foundation and the  
21 DAMOCLES European Union 6<sup>th</sup> Framework Program Integrated Research Project. The  
22 Swedish Polar Research Secretariat (SPRS) provided access to the icebreaker *Oden* and  
23 logistical support. Michael Tjernström is specifically thanked for his co-coordination of  
24 ASCOS. We are grateful to the SPRS logistical staff and to *Oden's* Captain Mattias Peterson  
25 and his crew. ASCOS is an IPY project under the AICIA-IPY umbrella and an endorsed  
26 SOLAS project. The Swedish Research Council (VR), the Knut and Alice Wallenberg  
27 Foundation and the Bolin Centre for Climate Research at Stockholm University provided  
28 support for this work.

29

30

## 1 **References**

- 2 Abbatt, J. P. D., Broekhuizen, K., and Pradeep Kumar, P.: Cloud condensation nucleus  
3 activity of internally mixed ammonium sulfate/organic acid aerosol particles, *Atm. Env.*, 39  
4 (26), 4767–4778, 2005.
- 5 Bigg, E. K., Leck, C., and Nilsson, E.D.: Sudden changes in arctic atmospheric aerosol  
6 concentrations during summer and autumn. *Tellus* 48B, 254-271, 1996.
- 7 Bigg, E. K. and Leck, C.: Cloud-active particles over the central Arctic Ocean, *J. Geophys.*  
8 *Res.*, 106, 32,155-32, 166, 2001a.
- 9 Bigg, E. K. and Leck, C.: Properties of the aerosol over the central Arctic Ocean, *J. Geophys.*  
10 *Res.*, 106, 32101–32109, 2001b.
- 11 Bigg, E. K., Leck, C., and Nilsson, E. D.: Sudden changes in aerosol and gas concentrations  
12 in the central Arctic marine boundary layer: Causes and consequences, *J. Geophys. Res.*, 106,  
13 32167-32185, 2001.
- 14 Bigg, E. K., Leck, C., and Tranvik, T.: Particulates of the surface microlayer of open water in  
15 the central Arctic Ocean in summer, *Mar. Chem.*, 91, 131–141, 2004.
- 16 Bigg, E.K. and Leck, C.: The composition of fragments of bubbles bursting at the ocean  
17 surface, *J. Geophys. Res.*, 113 (D1), 1209, doi:10.1029/2007JD009078, 2008.
- 18 Birmili, W., Stratmann, F., and Wiedensohler, A.: Design of a DMA-based size spectrometer  
19 for a large particle size range and stable operation, *J. Aerosol Sci.*, 30, 549–553, 1999.
- 20 Chang, R. Y.-W., Leck, C., Graus, M., Müller, M., Paatero, J., Burkhart, J. F., Stohl, A., Orr,  
21 L. H., Hayden, K., Li, S.-M., Hansel, A., Tjernström, M., Leitch, W. R., and Abbatt, J. P. D.:  
22 Aerosol composition and sources in the central Arctic Ocean during ASCOS, *Atmos. Chem.*  
23 *Phys.*, 11, 10619-10636, doi:10.5194/acp-11-10619-2011, 2011.
- 24 Chuang, P.: Measurement of the timescale of hygroscopic growth for atmospheric aerosols, *J.*  
25 *Geophys. Res.*, 108, D9, 4282, doi:10.1029/2002JD002757, 2003.
- 26 Davis, E. J.: A history and state-of-the-art of accommodation coefficients, *Atmospheric*  
27 *Research*, 82 (3-4), 561-578, 2006.
- 28 Draxler, R. R. and Rolph, G. D.: HYSPLIT (HYbrid Single-Particle Lagrangian Integrated  
29 Trajectory) Model access via NOAA ARL READY Website, available at:

1 <http://ready.arl.noaa.gov/HYSPLIT.php> (last access: 7 April 2010), NOAA Air Resources  
2 Laboratory, Silver Spring, MD, 2011.

3 EANET (Acid Deposition Monitoring Network in East Asia): Report of the Inter-Laboratory  
4 Comparison Project 2007, available at: <http://www.eanet.asia/product/>, 2008.

5 Fu, P., Kawamura, K., Chen, J., and Barrie, L. A.: Isoprene, Monoterpene, and Sesquiterpene  
6 Oxidation Products in the High Arctic Aerosols during Late Winter to Early Summer,  
7 *Environ. Sci. Technol.*, 43 (11), 4022-4028, 2009.

8 Gao, Q., Leck, C., Rauschenberg, C., and Matrai, P.A.: On the chemical dynamics of  
9 extracellular polysaccharides in the high Arctic surface microlayer, *Ocean Sci. Discuss.* 9,  
10 215–259, 2012.

11 Hamacher-Barth, E., Jansson, K. and Leck, C.: A method for sizing submicrometer particles  
12 in air collected on Formvar films and imaged by scanning electron microscope *Atmos. Meas.*  
13 *Tech.*, 6, 1-16, 2013.

14 Hede, T., Xin, L. T., Tu, Y., Leck, C. and Ågren, H.: 2011, HULIS in nano aerosol clusters;  
15 investigations of surface tension and aggregate formation using Molecular Dynamics  
16 simulations, *Atmos. Chem. Phys.*, 11(13): 6549-6557.v., 2011.

17 Heintzenberg, J., Birmili, W., Wiedensohler, A., Nowak, A., and Tuch, T.: Structure,  
18 variability and persistence of the submicrometer marine aerosol, *Tellus* 56B, 4, 357-367,  
19 2004.

20 Heintzenberg, J., Leck, C., Birmili, W., Wehner, B., Tjernström, M., and Wiedensohler, A.:  
21 Aerosol number-size distributions during clear and fog periods in the summer high Arctic:  
22 1991, 1996 and 2001, *Tellus*, 58B, 41-50, 2006.

23 Heintzenberg, J. and Leck, C.: The summer aerosol in the central Arctic 1991–2008: did it  
24 change or not?, *Atmos. Chem. Phys.*, 12, 3969–3983, doi:10.5194/acp-12-3969-2012, 2012.

25 Herman G., and Goody, R.: Formation and persistence of summertime Arctic stratus clouds,  
26 *J. Atmos. Sci.*, 33, 1537-1553, 1976.

27 Hinds, W. C.: *Aerosol Technology: Properties, Behavior, and Measurement of Airborne*  
28 *Particles*, Wiley-Interscience, 504pp., ISBN: 978-0-471-19410-1, 1999.

- 1 Hoppel, W. A., Frick, G. M., and Larson, R. E.: Effect of nonprecipitating clouds on the  
2 aerosol size distribution in the marine boundary layer, *Geophys. Res. Lett.*, 13, 125-128,  
3 1986.
- 4 Hoppel, W.A., Frick, G.M., Fitzgerald, J.W., and Larson, R.E.: Marine boundary layer  
5 measurements of new particle formation and the effects non precipitating clouds have on  
6 aerosol size distribution, *J. Geophys. Res.*, 99, 14443-14459, doi: 10.1029/94JD00797, 1994.
- 7 Intrieri, J. M., Fairall, C. W., Shupe, M. D., Persson, P. O. G., Andreas, E. L., Guest, P. S.,  
8 and Moritz, R. E.: An annual cycle of Arctic surface cloud forcing at SHEBA, *J. Geophys.*  
9 *Res.*, 107, 8039, doi:10.1029/2000JC000439, 2002.
- 10 Karl, M., Gross, A., Leck, C., and Pirjola, L.: A new flexible multicomponent model for the  
11 study of aerosol dynamics in the marine boundary layer, *Tellus B*, 63, 1001–1025, 2011.
- 12 Karl, M., Leck, C., Gross, A., and Pirjola, L.: A study of new particle formation in the marine  
13 boundary layer over the central Arctic Ocean using a flexible multicomponent aerosol  
14 dynamic model, *Tellus B*, 64, 17158, doi:10.3402/tellusb.v64i0.17158, 2012.
- 15 Karl, M., Leck, C., Coz, E., and Heintzenberg, J.: Marine nanogels as a source of atmospheric  
16 nanoparticles in the high Arctic. *Geophys. Res. Lett.*, 40, 3738-3743, doi:10.1002/grl.50661,  
17 2013.
- 18 Kay, J. E., and Gettelman, A.: Cloud influence on and response to seasonal Arctic sea ice  
19 loss, *J. Geophys. Res.*, 114, D18204, doi:10.1029/2009JD011773, 2009.
- 20 Kerminen, V.-M. and Leck, C.: Sulfur chemistry over the central Arctic Ocean during the  
21 summer: Gas-to-particle transformation, *J. Geophys. Res.*, 106, 32087-32099, 2001.
- 22 Kupiszewski, P., Leck, C., Tjernström, M., Sjogren, S., Sedlar, J., Graus, M., Müller, M.,  
23 Brooks, B., Swietlicki, E., Norris, S., and Hansel, A.: Vertical profiling of aerosol particles  
24 and trace gases over the central Arctic Ocean during summer, *Atmos. Chem. Phys.*, 13,  
25 12405–12431, doi:10.5194/acp-13-12405-2013, 2013.
- 26 Köhler, H.: The nucleus in and the growth of hygroscopic droplets. *T. Faraday Soc.*, 32, 1152-  
27 1161, 1936.
- 28 Lannefors, H., Heintzenberg, J., and Hansson, H.-C.: A comprehensive study of physical and  
29 chemical parameters of the Arctic summer aerosol; results from the Swedish expedition  
30 Ymer-80, *Tellus 35B*, 40–54, 1983.

- 1 Leaitch, W. R., Strapp, J. W., Isaac, G. A.: Cloud droplet nucleation and cloud scavenging of  
2 aerosol sulfate in polluted atmospheres, *Tellus*, 38B, 328-344, 1986.
- 3 Leck, C. and Persson, C.: Seasonal and short-term variability in dimethyl sulfide, sulfur  
4 dioxide and biogenic sulfur and sea salt aerosol particles in the arctic marine boundary layer,  
5 during summer and autumn, *Tellus* 48B, 272-299, 1996.
- 6 Leck, C., Bigg, E. K., Covert, D. S., Heintzenberg, J., Maenhaut, W., Nilsson, E. D., and  
7 Wiedensohler, A.: Overview of the atmospheric research program during the International  
8 Arctic Ocean Expedition of 1991 (IAOE-91) and its scientific results, *Tellus*, 48B, 136-155,  
9 1996.
- 10 Leck, C. and Bigg, E. K.: Aerosol production over remote marine areas - A new route,  
11 *Geophys. Res. Lett.*, 23, 3577-3581, 1999.
- 12 Leck, C., Nilsson, E. D., Bigg, E. K., and Bäcklin, L.: Atmospheric program on the Arctic  
13 Ocean Expedition 1996 (AOE-96): an overview of scientific goals, experimental approaches,  
14 and instruments, *J. Geophys. Res.*, 106, 32051–32067, 2001.
- 15 Leck, C., Norman, M., Bigg, E. K., and Hillamo, R.: Chemical composition and sources of  
16 the high Arctic aerosol relevant for cloud formation, *J. Geophys. Res.*, 107, 4135,  
17 doi:10.1029/2001JD001463, 2002.
- 18 Leck, C., Tjernström, M., Matrai, P., Swietlicki, E., and Bigg, K.: Can marine micro-  
19 organisms influence melting of the Arctic pack ice?, *EOS T. Am. Geophys. Un.*, 85, 25–32,  
20 doi:10.1029/2004EO030001, 2004.
- 21 Leck, C., and Bigg, E. K.: Biogenic particles in the surface microlayer and overlaying  
22 atmosphere in the central Arctic Ocean during summer, *Tellus* 57B, 305-316, 2005a.
- 23 Leck, C., and Bigg, E. K.: Evolution of the marine aerosol – A new perspective. *Geophys.*,  
24 *Res., Lett.*, 32, L19803. doi: 10.1029/2005GL023651, 2005b.
- 25 Leck, C., and Bigg, E. K.: New particle formation of marine biological origin, *Aerosol*  
26 *Science and Technology*, 44, 570–577, 2010.
- 27 Leck, C., Gao, Q., Mashayekhy Rad, F., and Nilsson, U.: Size resolved airborne particulate  
28 polysaccharides in summer high Atmos. *Chem. Phys.*, 13, 12573–12588, 2013.

1 Lelieveld, J. and Heintzenberg, J.: Sulfate cooling effect on climate through in-cloud  
2 oxidation of anthropogenic SO<sub>2</sub>, *Science* 258, 117-120, 1992.

3 Lohmann, U. and Leck, C.: Importance of submicron surface-active organic aerosols for  
4 pristine Arctic clouds, *Tellus*, 57B, 261-268, 2005.

5 Martin, M., Chang, R. Y.-W., Sierau, B., Sjögren, S., Swietlicki, E., Abbatt, J. P. D., Leck, C  
6 and Lohmann U.: Cloud condensation nuclei closure study on summer arctic aerosol, *Atmos.*  
7 *Chem. Phys.*, 11, 11335-11350, 2011.

8 Mauritsen, T., Sedlar, J., Tjernström, M., Leck, C., Martin, M., Shupe, M., Sjogren, S.,  
9 Sierau, B., Persson, P. O. G., Brooks, I. M., and Swietlicki, E.: An Arctic CCN-limited cloud-  
10 aerosol regime, *Atmos. Chem. Phys.*, 11, 165-173, doi:10.5194/acp-11-165-2011, 2011.

11 Morita, A., Sugiyama, M., Kameda, H., Koda, S., Hanson, D. R.: Mass Accommodation  
12 Coefficient of Water: Molecular Dynamics Simulation and Revised Analysis of Droplet  
13 Train/Flow Reactor Experiment, *J. Phys. Chem. B.*, 108 (26), 9111–9120, 2004.

14 Narukawa, M., Kawamura, K., Li, S.-M., and Bottenheim, J. W.: Dicarboxylic acids in the  
15 Arctic aerosols and snowpacks collected during ALERT 2000, *Atmos. Environ.*, 36, 2491-  
16 2499, 2002.

17 Nilsson, E.D., Rannik, Ü., Swietlicki, E., Leck, C., Aalto, P.P., Norman, M., and Zhou, J.:  
18 Turbulent aerosol number fluxes during the Arctic Ocean Expedition 1996, part II: a wind  
19 driven source of sub micrometere aerosol particles from the sea, *J. Geophys. Res.*, 106 (D23),  
20 32,139-32,154, 2001.

21 Norris, S. J., Brooks, I. M., de Leeuw, G., Sirevaag, A., Leck, C., Brooks, B. J., Birch, C. E.,  
22 and Tjernstrom, M.: Measurements of bubbles size spectra within Leeds in the Arctic summer  
23 pack ice, *Ocean Science*, 7, pp. 1-11, doi:10.5194/os-7-1-2011, 2011.

24 Ovadnevaite, J., Ceburnis, D., Martucci, G., Bialek, J., Monahan, C., Rinaldi, M., Facchini,  
25 M. C., Berresheim, H., Worsnop, D. R., and O’Dowd, C.: Primary marine organic aerosol: A  
26 dichotomy of low hygroscopicity and high CCN activity, *Geophys. Res. Lett.*, 38, L21806,  
27 doi:10.1029/2011GL048869, 2011.

28 Orellana, M. V., Matrai, P. A., Leck, C., Rauschenberg, C. D., Lee, A. M., and Coz, E.:  
29 Marine microgels as a source of cloud condensation nuclei in the high Arctic, *PNAS*, 108,  
30 13612–13617, 2011.

1 Paatero, J., Vaattovaara, P., Vestenius, M., Meinander, O., Makkonen, U., Kivi, R.,  
2 Hyvärinen, A., Asmi, E., Tjernström, M., and Leck, C.: Finnish contribution to the Arctic  
3 Summer Cloud Ocean Study (ASCOS) expedition, Arctic Ocean 2008, *Geophysica*, 45, 119-  
4 146, 2009.

5 Petters, M. D. and Kreidenweis, S. M.: A single parameter representation of hygroscopic  
6 growth and cloud condensation nucleus activity, *Atmos. Chem. Phys.*, 7, 1961-1971,  
7 doi:10.5194/acp-7-1961-2007, 2007.

8 Pruppacher, H. R. and Klett, J. D.: *Microphysics of Clouds and Precipitation*, Kluwer  
9 Academic Publishers, Dordrecht, 1997.

10 Roberts, G. C. and Nenes, A.: A continuous-flow stream wise thermal-gradient CCN chamber  
11 for atmospheric measurements, *Aerosol Sci. Technol.*, 39, 206–221,  
12 doi:10.1080/027868290913988, 2005.

13 Ruehl, C. R., Chuang, P. Y., and Nenes, A.: How quickly do cloud droplets form on  
14 atmospheric particles?, *Atmos. Chem. Phys.*, 8, 1043-1055, doi:10.5194/acp-8-1043-2008,  
15 2008.

16 Sedlar, J., Tjernström, M., Mauritsen, T., Shupe, M. D., Brooks, I. M., Persson, P. O. G.,  
17 Birch, C. E., Leck, C., Sirevaag, A., and Nicolaus, M.: A transitioning Arctic surface energy  
18 budget: the impacts of solar zenith angle, surface albedo and cloud radiative forcing, *Clim.*  
19 *Dynam.*, 37, 1643–1660, doi:10.1007/s00382-010-0937-5, 2011.

20 Shantz, N. C., Chang, R. Y.-W., Slowik, J. G., Vlasenko, A., Abbatt, J. P. D., and Leitch, W.  
21 R.: Slower CCN growth kinetics of anthropogenic aerosol compared to biogenic aerosol  
22 observed at a rural site, *Atmos. Chem. Phys.*, 10, 299-312, doi:10.5194/acp-10-299-2010,  
23 2010.

24 Shupe, M. D., Persson, P. O. G., Brooks, I. M., Tjernström, M., Sedlar, J., Mauritsen, T.,  
25 Sjogren, S., and Leck, C.: Cloud and boundary layer interactions over the Arctic sea ice in  
26 late summer, *Atmos. Chem. Phys.*, 13, 9379–9399, doi:10.5194/acp-13-9379-2013, 2013.

27 Sierau, B., Chang, R. Y.-W., Leck, C., Paatero, J., and Lohmann, U.: Single-particle  
28 characterization of the high-Arctic summertime aerosol, *Atmos. Chem. Phys.*, 14, 7409–7430,  
29 doi:10.5194/acp-14-7409-2014, 2014.

1 Svenningsson, B., Rissler, J., Swietlicki, E., Mircea, M., Bilde, M., Facchini, M. C., Decesari,  
2 S., Fuzzi, S., Zhou, J., Mønster, J., and Rosenørn, T.: Hygroscopic growth and critical  
3 supersaturations for mixed aerosol particles of inorganic and organic compounds of  
4 atmospheric relevance, *Atmos. Chem. Phys.*, 6, 1937-1952, doi:10.5194/acp-6-1937-2006,  
5 2006.

6 Takahama, S., and Russell, L. M.: A molecular dynamics study of water mass  
7 accommodation on condensed phase water coated by fatty acid monolayers, *J. Geophys. Res.*,  
8 116, D02203, doi:10.1029/2010JD014842, 2011.

9 Tjernström, M., Leck, C., Persson, P. O., Jensen, M., Oncley, S. and Targino, A.: The  
10 Summertime Arctic Atmosphere: Meteorological measurements during the Arctic Ocean  
11 Experiment 2001 (AOE-2001), *Bulletin of the American Meteorological Society*, 85, 1305 -  
12 1321, 2004.

13 Tjernström, M., Sedlar, J., and Shupe, M. D.: How well do regional climate models reproduce  
14 radiation and clouds in the Arctic?, *J. Appl. Meteorol. Clim.*, 47, 2405–2422, 2008.

15 Tjernström, M., Birch, C. E., Brooks, I. M., Shupe, M. D., Persson, P. O. G., Sedlar, J.,  
16 Mauritsen, T., Leck, C., Paatero, J., Szczodrak, M. And Wheeler, C. R.: Meteorological  
17 conditions in the central Arctic summer during the Arctic Summer Cloud Ocean Study  
18 (ASCOS), *Atmos. Chem. Phys.*, 12, 6863-6889, 2012.

19 Tjernström, M., Leck, C., Birch, C. E., Brooks, B. J., Brooks, I. M., Bäcklin, L., Chang, R.  
20 Y.-W., Granath, E., Graus, M., Hansel, A., Heintzenberg, J., Held, A., Hind, A., de la Rosa,  
21 S., Johnston, P., Knulst, J., de Leeuw, G., Di Liberto, L., Martin, M., Matrai, P. A., Mauritsen,  
22 T., Müller, M., Norris, S. J., Orellana, M. V., Orsini, D. A., Paatero, J., Persson, P. O. G.,  
23 Gao, Q., Rauschenberg, C., Ristovski, Z., Sedlar, J., Shupe, M. D., Sierau, B., Sirevaag, A.,  
24 Sjogren, S., Stetzer, O., Swietlicki, E., Szczodrak, M., Vaattovaara P., Wahlberg, N.,  
25 Westberg, M., and Wheeler, C. R.: The Arctic Summer Cloud-Ocean Study (ASCOS):  
26 overview and experimental design, *Atmos. Chem. Phys.*, 14, 2823-2869, 2014.

27 Tuckermann, R.: Surface tension of aqueous solutions of water-soluble organic and inorganic  
28 compounds, *Atmos. Env.*, 41, 6265–6275, 2007.

29 Twomey, S.: Pollution and the planetary albedo, *Atmos. Env.*, 8 (12), 1251–1256, 1974.



- 1 Verdugo, P.: Marine Microgels, *Ann. Rev. Marine Sci.*, 4, 375-400, DOI: 10.1146/annurev-  
2 marine-120709-142759, 2011.
- 3 Walsh, J., Kattsov, V., Chapman, W., Govorkova, V., and Pavlova, T.: Comparison of Arctic  
4 climate simulations by uncoupled and coupled global models, *J. Climate*, 15, 1429-1446,  
5 2002.
- 6 Winkler, P. M., Vrtala A., Wagner, P. E., Kulmala, M., Lehtinen, K. E. J., and Vesala, T.:  
7 Mass and Thermal Accommodation during Gas-Liquid Condensation of Water, *Phys. Rev.*  
8 *Let.*, 93, 7, 075701-1– 075701-4, 2004.
- 9 Winkler, P. M., Vrtala, A., Rudolf, R., Wagner, P. E., Riipinen, I., Vesala, T., Lehtinen, K. E.  
10 J., Viisanen, Y., and Kulmala, M.: Condensation of water vapor: Experimental determination  
11 of mass and thermal accommodation coefficients, *J. Geophys. Res.*, 111, D19202,  
12 doi:10.1029/2006JD007194, 2006.
- 13 Xin Li, Leck, C, Sun, L, Hede, T, Tu, Y, and Ågren, H.: Cross-Linked Polysaccharide  
14 Assemblies in Marine Gels: An Atomistic Simulation, *Journal of Physical Chemistry Letters*,  
15 4, 2637–2642, dx.doi.org/10.1021/jz401276r, 2013.
- 16 Zhou, J., Swietlicki, E., Berg, O. H., Aalto, P. P., Hämeri, K., Nilsson E. D., and Leck, C.:  
17 Hygroscopic properties of aerosol particles over the central Arctic Ocean during summer, *J.*  
18 *Geophys. Res.*, 106, 32111-32 123, 2001.
- 19

1 Table 1. The 25<sup>th</sup>, 50<sup>th</sup> (median) and 75<sup>th</sup> percentile aerosol number concentrations seen by the TDMS for 40, 80 and 300 nm diameter sizes  
 2 separately for the impactor samples at the marginal ice zone (MIZ-1) and over the pack ice (PI-1, 8,10, 13, and 15). Values are at STP. Also  
 3 listed is the information on sampling start – stop times of the impactors.  
 4

Sample	Start time	End time	N <sub>40 nm</sub>			N <sub>80 nm</sub>			N <sub>300 nm</sub>		
	(UTC)	(UTC)	50% percentile cm <sup>-3</sup>	25% percentile cm <sup>-3</sup>	75% percentile cm <sup>-3</sup>	50% percentile cm <sup>-3</sup>	25% percentile cm <sup>-3</sup>	75% percentile cm <sup>-3</sup>	50% percentile cm <sup>-3</sup>	25% percentile cm <sup>-3</sup>	75% percentile cm <sup>-3</sup>
	DOY	DOY									
MIZ-1	217.503	218.508	704	536	806	110	90	126	15	9.5	23
PI-1	225.967	227.321	49	31	121	32	10	63	3.3	1.3	7.3
PI-8	235.049	236.253	932	855	1094	190	144	216	1.4	0.39	5.1
PI-10	237.625	238.271	47	20	61	54	20	89	3.8	2.4	5.6
PI-15	244.826	245.977	0.90	0.55	2.2	0.97	0.25	2.8	0.60	0.02	1.8

5  
 6  
 7

1 Table 2. The 25<sup>th</sup>, 50<sup>th</sup> (median) and 75<sup>th</sup> percentile CCNC separately for open water (OW-1), marginal ice zone (MIZ-1) and pack ice (PI-1, 3, 6,  
 2 8, 9, 10, 13, and 15) measurements at 0.2 % SS (counter 1). Values are at STP. Also listed are information on sampling start – stop times and  
 3 sample duration and of the air trajectory cluster and average DOI during the sampling time for each of the impactors.







4

Sample	Start time DOY	End time DOY	Sampling location	Trajectory -cluster	DOI	CCNC 50% percentile cm <sup>-3</sup>	CCNC 25% percentile cm <sup>-3</sup>	CCNC 75% percentile cm <sup>-3</sup>	Missing aerosol fraction
OW-1	216.561	217.342	Open water	-	N/A	12.9	8.2	24.6	0.51
MIZ-1	217.503	218.508	Marginal ice zone	-	0	57.3	33.5	70.2	0.67
PI-1	225.967	227.321	Ice drift	1	2.5	17.4	1.8	31.7	0.46
PI-3	228.656	229.626	Ice drift	2	1.6	23.8	6.4	52.7	0.68
PI-6	232.272	233.269	Ice drift	1	4.6	29.4	15.5	45.7	0.68
PI-8	235.049	236.253	Ice drift	3	N/A	13.0	6.9	16.8	0.40
PI-9	236.382	237.419	Ice drift	2	1.2	30.1	25.8	32.8	0.56
PI-10	237.625	238.271	Ice drift	2	1.4	23.8	15.5	41.4	0.31
PI-13	240.708	242.700	Ice drift	4	6.1	44.3	30.9	47.9	0.76
PI-15	216.561	217.342	Ice drift	5	9.3	0.95	0.40	2.1	0.57

5



1 Table 3. Assumptions on the missing non-water soluble aerosol fraction used in the simulations. The droplet bulks show increasing ionic  
 2 concentration moving from gray to blue. Orange and red droplet fringes show various degrees of depressions in surface tension, red being the  
 3 strongest. Gray diamonds represent a core of water-insoluble particle.

4

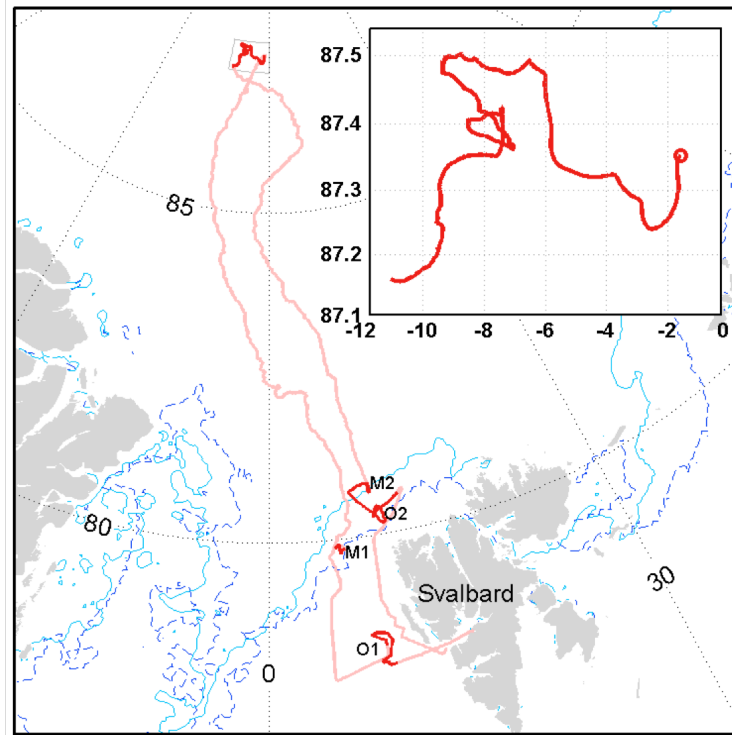
Simulation	Illustration	Description
AD		Missing fraction behaves like internally mixed adipic acid; low water-solubility and moderate surface active.
PIN		Missing fraction behaves like internally mixed cis-pinonic acid; low water-solubility and highly surface active.
INSOL		Missing fraction behaves like a water-insoluble particle inside the droplets; no surface activity.
SOL		Missing fraction is assumed to be non-existent, only the determined chemical size distribution is used.
AD_ext		The analyzed part is externally mixed with an aerosol consisting of adipic acid.
PIN_ext		The analyzed part is externally mixed with an aerosol consisting of cis-pinonic acid.

1 Table 4. Assumptions on the missing non-water soluble aerosol fraction used in the simulations. with modified condensation accommodation  
2 coefficients.

3

Simulation	Illustration	Description
AC1		As the AD case, but with the condensation-accommodation coefficient set to $10^{-4}$ .
AC2		As the AD case, but with a variable condensation-accommodation coefficient, see text for details.

4



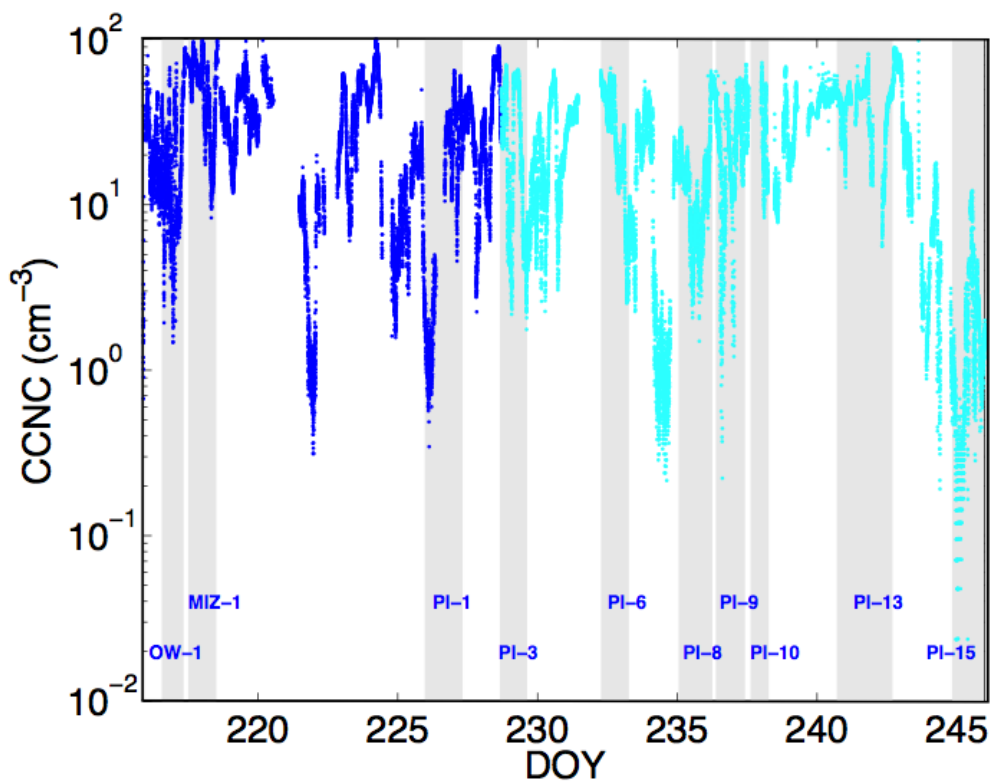
1

2 Figure 1. Map of the ASCOS cruise track (pink) with ice-drift period (PI-drift) highlighted  
 3 (red) and (inset) shown in detail with the start of the drift marked by the circle. The left-hand  
 4 part of the track shows the initial northward track while the right-hand track shows the  
 5 southward, return track. Convoluted track lines in open water, OW (O1 & O2) and at the ice  
 6 edge, MIZ (M1 & M2) are associated with shorter sampling stations. The dashed light blue  
 7 line illustrates the ice edge at the time of entry and the darker blue line at the time of exit.

8

9

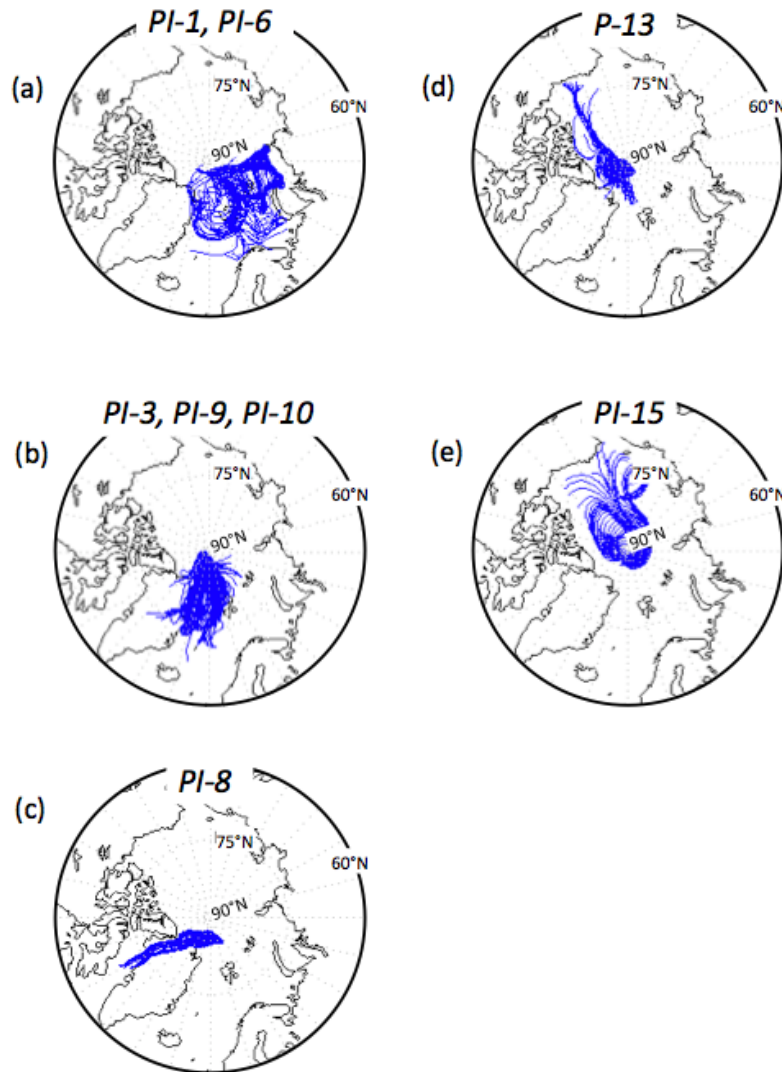
10



1  
 2 Figure 2. CCNC as a function of time in units of  $\text{cm}^{-3}$ . Blue dots show CCNC measured at  
 3 0.17% water vapor SS, while light blue dots show the CCNC at 0.21% water vapor  
 4 supersaturation. The grey shaded bars mark the duration of each of the impactor samples.  
 5 Details on impactor start and stop times are given in Table 2.

6  
 7  
 8  
 9  
 10  
 11  
 12  
 13  
 14  
 15

1

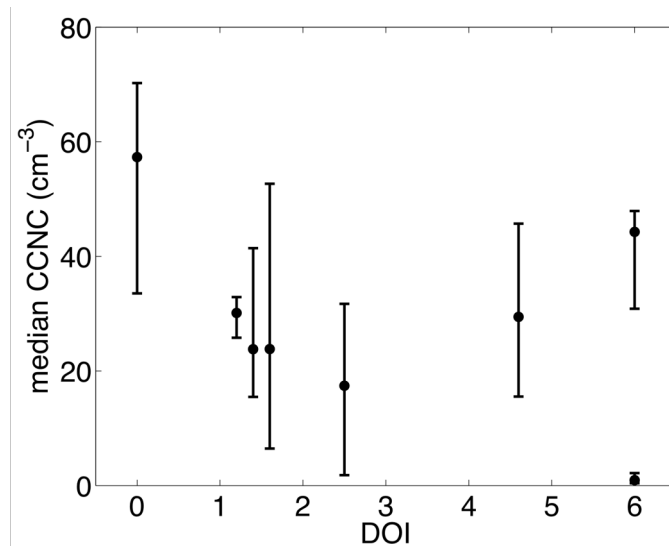


2

3

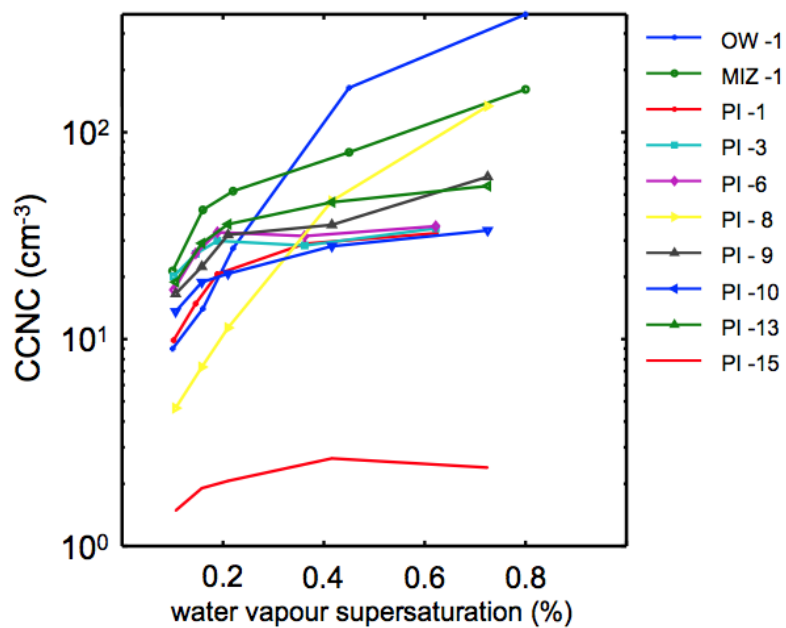
4 **Figure 3.** Air trajectory clusters with an arrival height of 100 m at the position of the  
5 icebreaker during: (a) cluster 1 (DOY 227, DOY 229-232) originated easterly from the  
6 Barents - and Kara Seas, (b) cluster 2 (DOY 228, DOY 236, 238-239) from the Greenland  
7 Sea- Fram Strait area, (c) cluster 3 (DOY 234-235) from Greenland, (d) cluster 4 from north-  
8 western circumpolar over the pack ice during DOY 240-243, and (e) cluster 5 from north-  
9 western circumpolar over the pack ice during DOY 243-246. **Table 2 gives the calculated**  
10 **DOI for each of the impactors.**





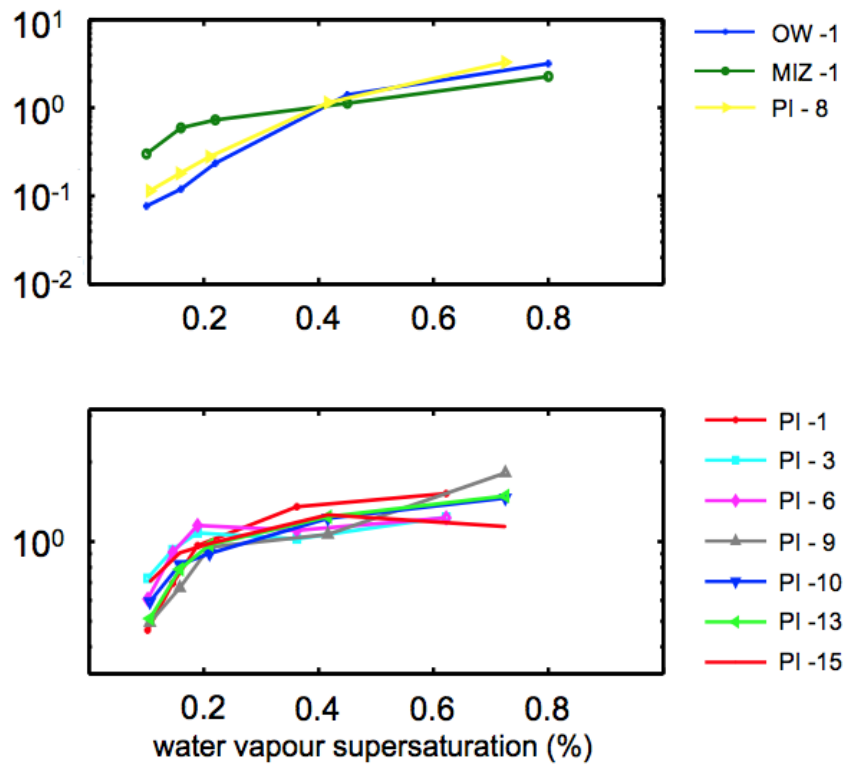
1  
2  
3  
4  
5  
6

Figure 4. Median (50<sup>th</sup> percentile) CCCNC for the duration of the impactor samples as a function of travel time over ice (DOI, days). Data for all travel times of five days and longer have been collected at 6 days. Error bars indicate 25<sup>th</sup> and 75<sup>th</sup> percentile.



7  
8  
9  
10  
11

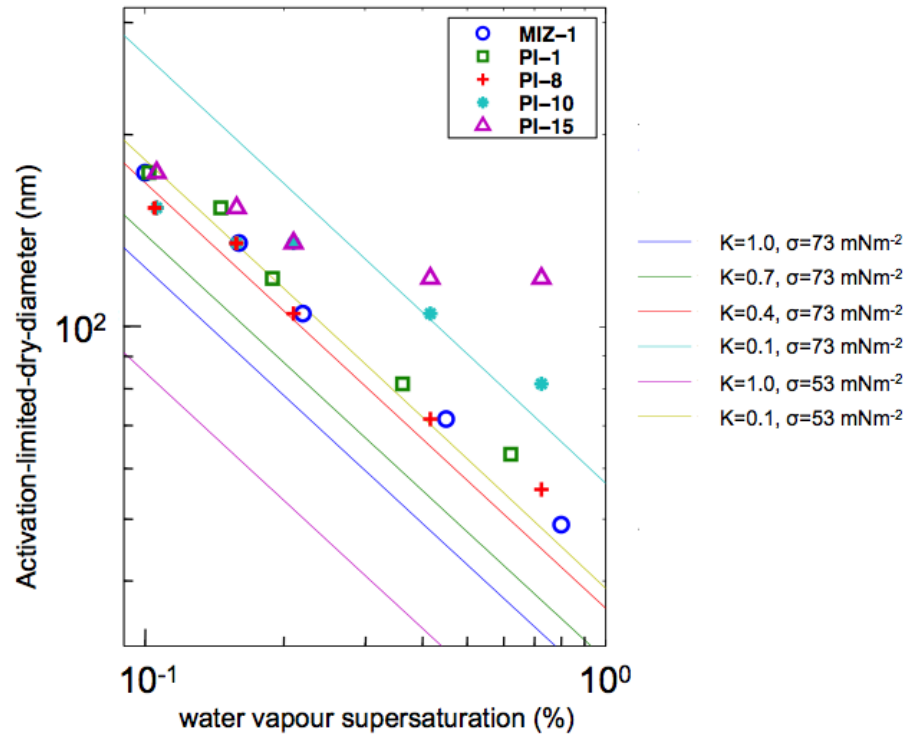
Figure 5. The measured CCNC as a function of the choice of water vapor SS (five levels between 0.1-0.8%) as seen by the second CCN sampler. The data is shown separately for open water (OW 1), marginal ice zone (MIZ 1) and pack ice (PI-1, 3, 6, 8, 9, 10, 13, and 15) measurements.



1

2 Figure 6. Variation in CCNC as a function of water vapor SS (as in Fig. 5) normalized to the  
 3 average CCNC value for the duration of the impactor samples.

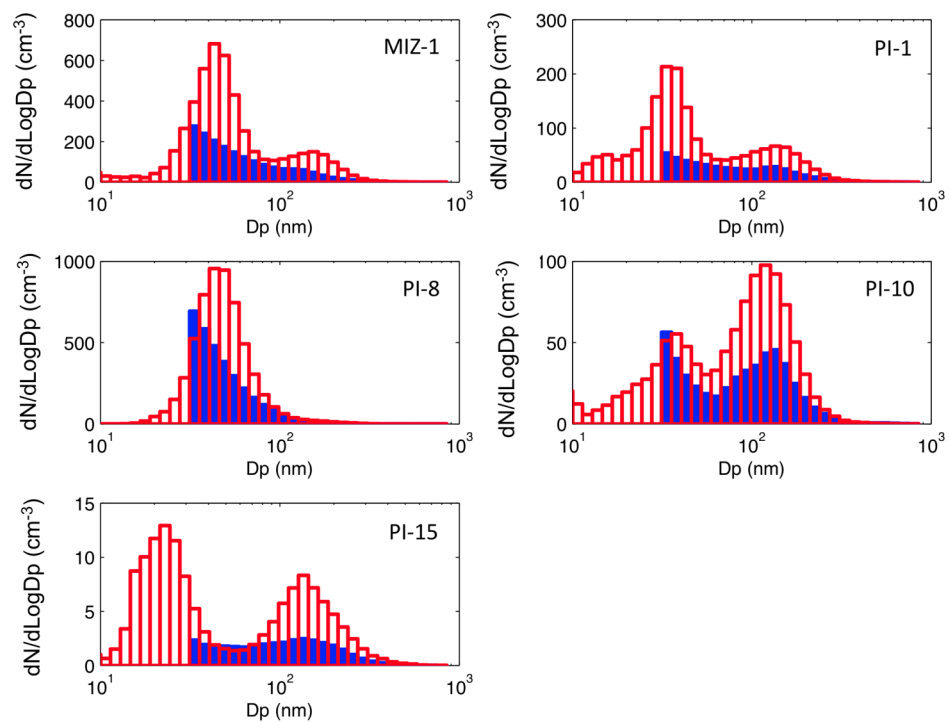
4



1

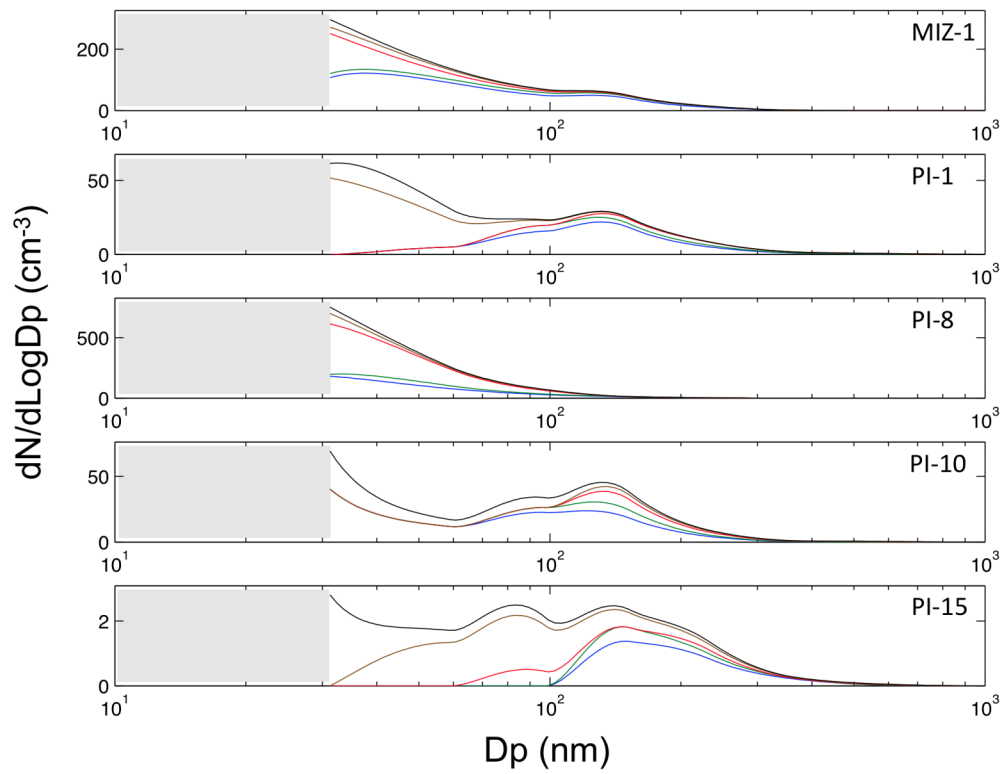
2 Figure 7.  $\kappa$ -Köhler theory predictions of the aerosol activation-limit-dry-diameter for assumed  
 3 pairs of  $\kappa$  and  $\sigma$  (lines) compared to values derived from the impactor samples MIZ-1, PI-1,  
 4 PI-8, PI-10 and PI-15 (dots).

5



1  
 2 Figure 8. Comparison between TDMPS number size distribution (red) and converted mass  
 3 size distributions (blue) for sample MIZ-1, PI-1, PI-8, PI-10 and PI-15.

4  
 5



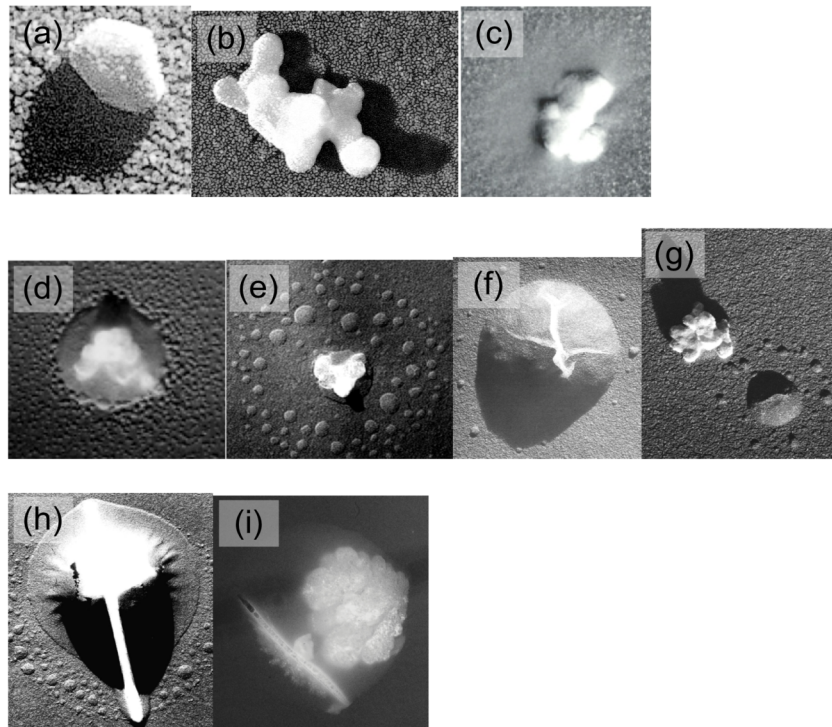
1

2 Figure 9. Number concentrations derived from impactor mass data. Blue line shows sulfate  
 3 only, green lines sulfate+MSA, red lines sulfate+MSA+Na<sup>+</sup>+Cl<sup>-</sup>, brown lines  
 4 sulfate+MSA+Na<sup>+</sup>+Cl<sup>-</sup>+Ca<sup>2+</sup>, and black lines show the total analyzed concentration.

5

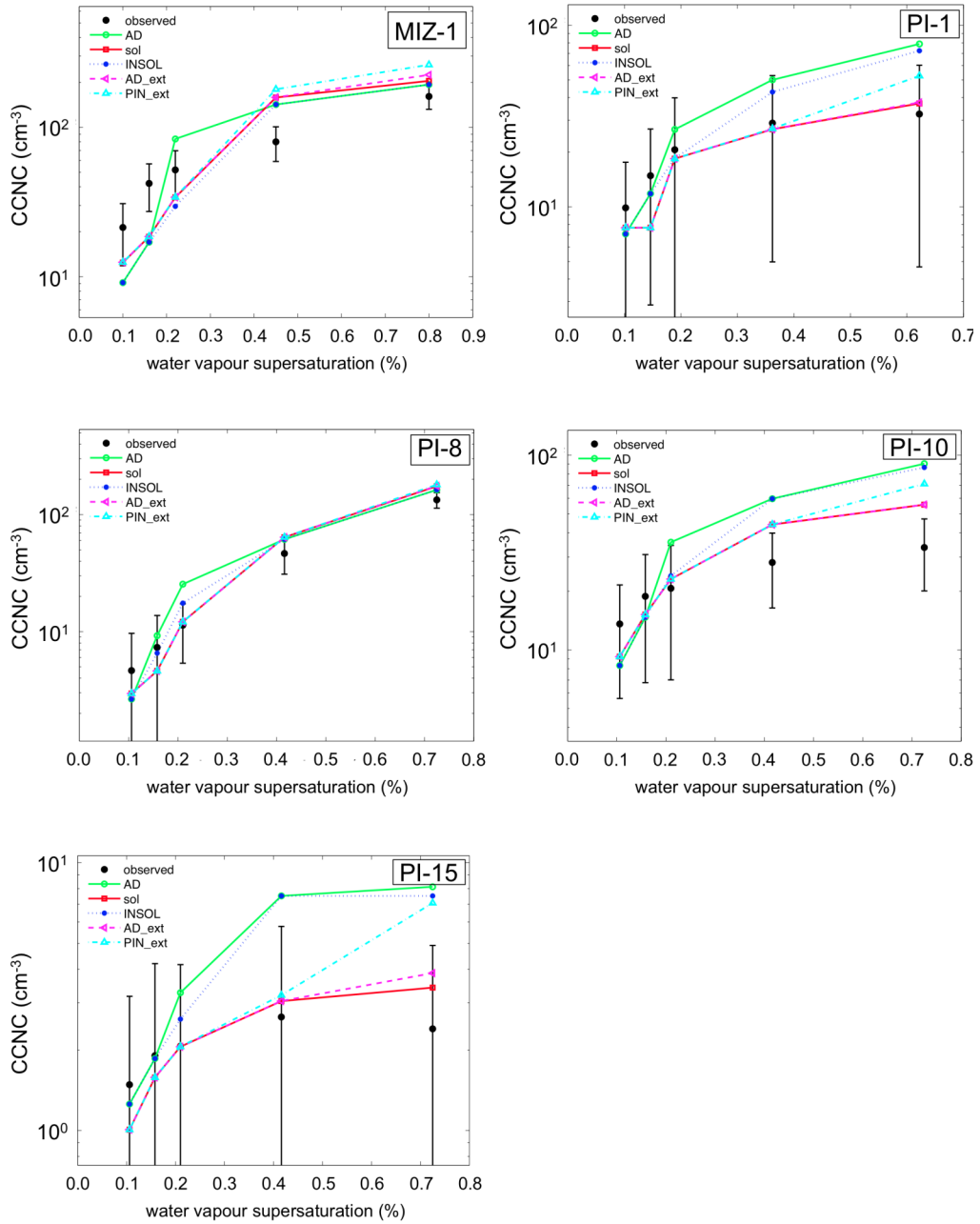
6

7



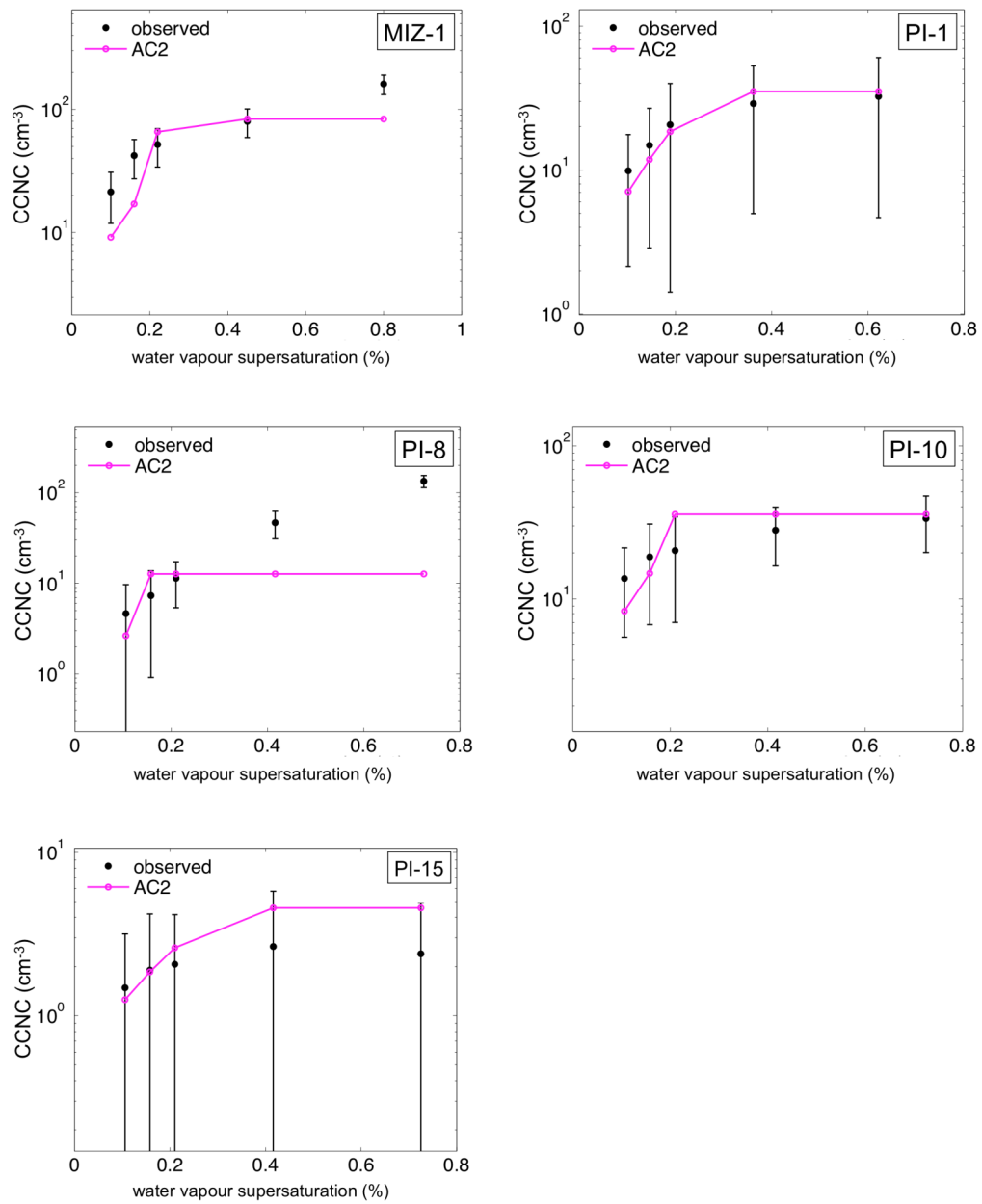
1  
 2 Figure 10. Examples of the changing nature of the high Arctic particles in different modal  
 3 diameters: a-c) sub-Aitken mode a: penta-hexagonal structure, crystalline and hydrophobic in  
 4 nature assumed to be a colloidal building block of a polymer gel, b: small polymer gel-  
 5 aggregate slightly covered with hydrophilic mucus, c: same as in b but with more mucus  
 6 remaining promoting its hydrophilic properties, d-g) Aitken to small accumulation mode, d:  
 7 particle with a high sulfuric acid content with a gel-aggregate inclusion embedded in a film of  
 8 high organic content, e: gel-aggregate with satellites, indicating the presence of organics and  
 9 acids, f: particle containing mainly ammonium sulfate and methane sulfonate, g: external  
 10 mixture of a gel-aggregate and similar particle as of f and h-i) large accumulation mode, h:  
 11 sea-salt particle with an organic content. The rod through its centre is assumed to be a  
 12 bacterium. The particle has an acquired coating of sulfuric acid., i: a gel- aggregate  
 13 containing a bacterium attached to a small aggregate possibly detached from the larger one.  
 14 The particles bubble like shape indicates a possible recent injection to the atmosphere at the  
 15 air sea interface.

16



1  
 2 Figure 11. Observed and simulated CCNC for sample MIZ-1, PI-1, PI-8, PI-10 and PI-15,  
 3 ranging from 0.1% to 0.8% water vapor SS. Error bars represent one standard deviation.

4



1  
 2 Figure 12. Observed and simulated CCNC for sample MIZ-1, PI-1, PI-8, PI-10 and PI-15,  
 3 ranging from 0.1% to 0.8% water vapor SS. Error bars represent one standard deviation. AC2  
 4 correspond to the assumption AD, see Table 2, with a variable condensation-accommodation  
 5 coefficient.